USDRIVE

DRIVING RESEARCH AND INNOVATION FOR VEHICLE EFFICIENCY AND ENERGY SUSTAINABILITY

U.S. DRIVE Highlights of Technical Accomplishments 2017

March 2018

U.S. DRIVE
Highlights of Technical Accomplishments Overview

Through precompetitive collaboration and technical exchange, U.S. DRIVE accelerates the development of energy-efficient advanced automotive and energy infrastructure technologies.

The U.S. DRIVE Partnership (*Driving Research for Vehicle efficiency and Energy sustainability*) is a voluntary government-industry partnership focused on precompetitive, advanced automotive and related infrastructure technology research and development (R&D). Partners are the United States Department of Energy (DOE); the United States Council for Automotive Research LLC (USCAR), a consortium composed of FCA US LLC, Ford Motor Company, and General Motors Company; five energy companies, (BP America, Chevron Corporation, Phillips 66 Company, ExxonMobil Corporation, and Shell Oil Products US); two electric utilities, DTE Energy and Southern California Edison; and the Electric Power Research Institute.

The Partnership benefits from a history of successful collaboration across multiple technical teams, each focused on a key area of the U.S. DRIVE portfolio (see below). These teams convene the best and brightest scientists and engineers from U.S. DRIVE partner organizations to discuss key technical challenges, identify possible solutions, and evaluate progress toward goals and targets published in technology roadmaps. U.S. DRIVE also has two working groups: one focused on fuels, recognizing an important opportunity to evaluate how various fuel properties can increase the efficiency of advanced internal combustion engines, and another related to energy efficient mobility systems, focused on understanding transportation system-level opportunities for significant energy savings in the movement of people and goods. By providing a framework for frequent and regular interaction among technical experts in common areas of expertise, the Partnership accelerates technical progress, helps to avoid duplication of efforts, ensures that publicly-funded research delivers high-value results, and overcomes high-risk barriers to technology commercialization.

U.S. DRIVE technical teams selected the highlights in this document from many hundreds of DOE-funded projects conducted by some of the nation's top research organizations in the field. Each one-page summary represents what DOE and automotive, energy, and utility industry partners collectively consider to be significant progress in the development of advanced automotive and infrastructure technologies. The report is organized by technical team area, with highlights in three general categories:

Vehicles

- Advanced Combustion and Emission Control
- Electrical and Electronics
- Electrochemical Energy Storage
- Fuel Cells
- Materials

Crosscutting

- Codes and Standards
- Grid Interaction
- Hydrogen Storage
- Integrated Systems Analysis

Fuels

- Fuel Pathway Integration
- Hydrogen Delivery
- Hydrogen Production

More information about U.S. DRIVE, including prior-year accomplishments reports and technology roadmaps, is available on the DOE (https://energy.gov/eere/vehicles/vehicle-technologies-office-us-drive) and USCAR (www.uscar.org) websites.

Table of Contents

VEHICLES

Advanced Combustion and Emission Control

2017 U.S. DRIVE Highlight

Low-Temperature Plasma Modeling Successfully Validated Against Experimental Observations

Advanced diagnostics and simulations provide OEMs with fundamental understanding and numerical tools to improve advanced ignition technologies that enable future high-efficiency engine strategies.

Argonne National Laboratory and Sandia National Laboratories

Increased charge dilution needed for future high-efficiency gasoline engine concepts demands a more robust ignition process. Low-temperature plasma (LTP) ignition is of interest to the automotive industry, due to the promotion of highly reactive chemical species such as atomic oxygen (O). However, LTP physics are poorly understood with no associated ignition models available in engine computational fluid dynamics (CFD) codes. A joint Argonne National Laboratory and Sandia National Laboratories effort led to successful LTP characterization and modeling. The team validated numerical results using a high-fidelity non-equilibrium plasma solver against complementary experimental data generated from nanosecond-pulsed high-voltage discharges. Main findings are as follows:

- Experiments mapped the LTP transition to an undesirable high-temperature arc as a function of ambient pressure, mixture composition, and electrode gap distance. Simulation results accurately matched the LTP-to-arc transition pressure boundaries with no model tuning.
- For LTP discharges, researchers observed thinner streamers and increased branching at higher ambient pressures. Simulations properly predicted branching ratios and streamer diameters (Figure 1).
- LTP-discharge gas heating was measured via calorimetry. The simulations indicate that the gas temperature increase was a result of electronic fast-gas heating from the LTP streamers (Figure 1).

Researchers compared experiments and simulations for a 5 mm gap and density values (1-5 kg/m^3) that are consistent with in-cylinder densities at typical part-load engine operation. Simulations accurately described the impact of operating conditions (e.g., pressure) on LTP chemical and thermal properties. Results are expected to lead to the development of an engineering LTP ignition model for engine simulations that can be leveraged to optimize ignition performance at specific engine operations.

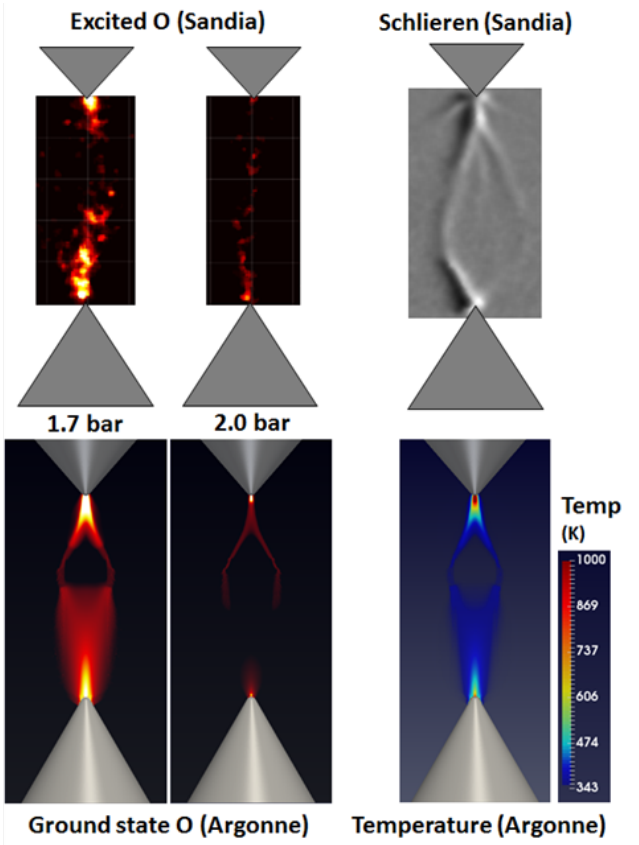

Figure 1. Qualitative comparison between experimental measurements and numerical predictions of chemical and thermal plasma properties (T = 343°K, pressure = 1.7-2.0 bar).

2017 U.S. DRIVE Highlight

On-Demand Blending of Gasoline and Natural Gas Offers up to 15% Engine Efficiency Improvement

Natural gas direct injection increases turbulence for better dilution tolerance and part-load efficiency while higher knock resistance enables increased full-load engine efficiency and a higher compression ratio.

Argonne National Laboratory, Ford Motor Company, and FCA US LLC

In current production natural gas (NG)/gasoline bi-fuel vehicles, fuels are supplied via port fuel injection (PFI). Injecting a gaseous fuel in the intake port significantly reduces the volumetric efficiency and consequently torque as compared to gasoline/E10. Direct injection (DI) of NG enhances the in-cylinder flow, mixing, and combustion process resulting in improved efficiency and performance.

A computational fluid dynamics (CFD) approach to model high-pressure gaseous injection was developed and validated against X-ray data from Argonne National Laboratory's Advanced Photon Source. Researchers experimentally assessed NG side and central DI of various designs and injection strategies along with CFD correlation. An improved understanding of the in-cylinder flow effects due to NG injection allowed the team to quantify and explain significant effects on combustion duration.

Side DI decreased the burn duration by up to 5° (Figure 1), allowing additional dilution and improved efficiency.

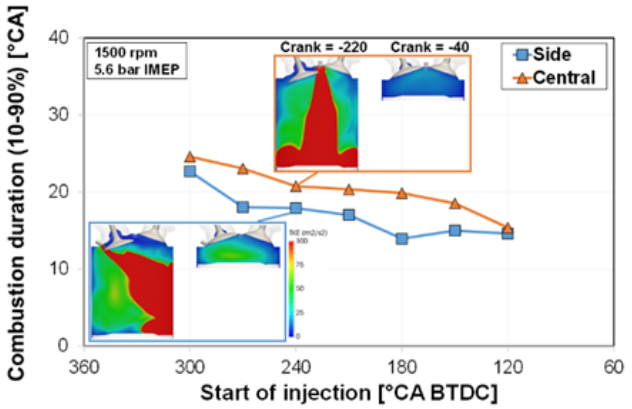

Figure 1. Measured combustion duration for side and central injector location with supporting turbulence plots from three-dimensional CFD depicting the impact of injector location on charge motion.

On-demand in-cylinder blending using E10 PFI and NG DI provides an additional lever to adjust in-cylinder turbulence as well as knock resistance across the entire engine speed and load range. NG DI improves part-load dilution tolerance due to higher in-cylinder turbulence and the high knock resistance of NG compared to E10 improves wide open throttle (WOT) performance and allows for increased compression ratio (CR) (Figure 2).

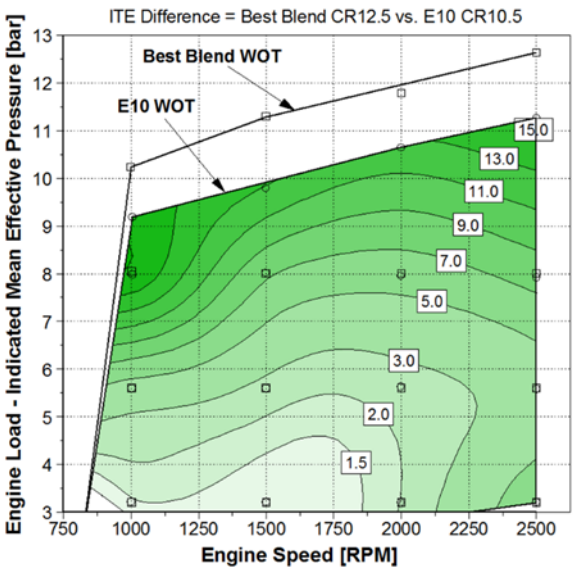

Figure 2. Indicated efficiency and peak load improvements with optimal NG/E10 blend at 12.5:1 CR compared to E10 baseline at 10.5:1 CR.

Vehicle level simulations suggest that implementing this strategy on a half-ton pickup truck with a naturally aspirated engine at 12.5:1 CR reduces carbon dioxide emissions on the aggressive US06 drive cycle by 27% (approximately half due to engine efficiency improvements and half due to reduced fuel carbon content) compared to E10 operation.

2017 U.S. DRIVE Highlight

Octane Blending Behavior Predicted for High-Octane Fuels in Gasoline within ± 3 Octane Units

Researchers made blending predictions using a newly developed chemical kinetic model for gasoline and high-octane fuels.

Lawrence Livermore National Laboratory

The ability to predict octane blending behavior of blendstocks in gasoline has been a challenge for half a century. Researchers have developed a chemical kinetic surrogate model for gasoline that can predict such blending effects for Co-Optima high-octane fuels in gasoline. These fuels increase research octane number (RON) and octane sensitivity (OS) in a base gasoline and enable high-efficiency, downsized, boosted, spark-ignition engine operation.

To achieve this, researchers improved the surrogate component kinetic submodels with updated rate constants from fundamental experiments and quantum chemistry calculations from the literature. The subcomponent models were further improved using new rapid compression machine (RCM) data from Argonne National Laboratory on iso-octane and a gasoline primary reference fuel (PRF90). Also, researchers used recent experimental ignition data from shock tubes and RCMs on n-heptane and toluene as validation targets.

Project researchers obtained RON and OS from ignition delay times (IDT) computed from the kinetic model using improved correlations developed at Lawrence Livermore National Laboratory (LLNL). These correlations relate IDT at 25 atm and 775K with RON and the slope of the IDT curve from 725-925K to OS. To obtain the results in Figure 1, researchers calculated about 1,000 IDTs using the Zero-RK fast chemistry solvers. As seen in Figure 1, the LLNL kinetic model and approach simulate the measured octane blending behavior of these fuels within ± 3 units. The demonstrated ability of the chemical kinetic model to simulate octane blending behavior and other fundamental combustion experiments gives LLNL researchers confidence in using the model for predicting and providing understanding of combustion behavior under boosted, downsized spark-ignition engine conditions.

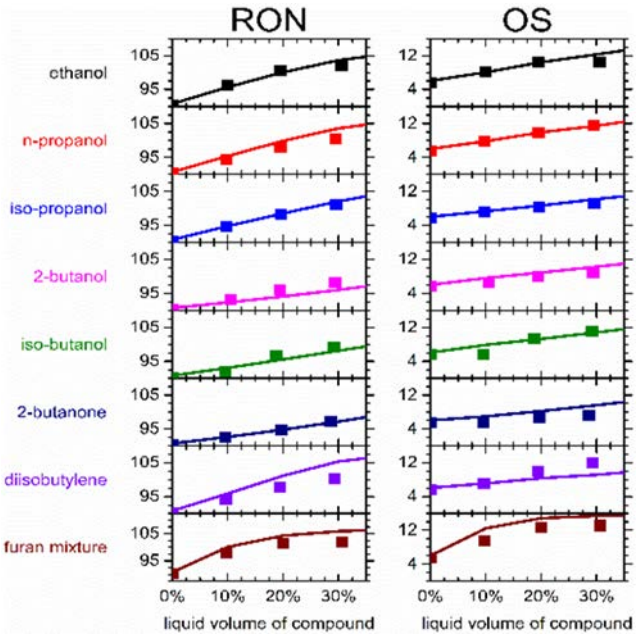

Figure 1. The predictions of octane blending of high-octane fuels in a 4-component base gasoline using the LLNL improved chemical kinetic model for gasoline (curves) compared to experimentally measured RON and OS obtained by the National Renewable Energy Laboratory (symbols).

2017 U.S. DRIVE Highlight

Fundamental Limitations Identified in Using Exhaust Gas Recirculation to Mitigate Knock

Study reveals kinetics-based reason for success of knock mitigation and higher efficiency for naturally-aspirated and lightly boosted engines.

Oak Ridge National Laboratory and Lawrence Livermore National Laboratory

Externally cooled exhaust gas recirculation (EGR) is an efficiency-increasing technology being deployed in some spark ignition (SI) engines to reduce pumping at light loads. Prior research shows EGR may enable further efficiency gains by mitigating knock at higher loads. However, the reported effectiveness of EGR to mitigate knock varies widely, especially in comparing boosted and naturally-aspirated (NA) engines. A collaboration between researchers at Oak Ridge National Laboratory and Lawrence Livermore National Laboratory provides a fundamental, kinetics-based explanation for the observed trends.

As the intake pressure changes for a given engine, so does the path of the unburned fuel and air mixture in the pressure-temperature (PT) domain, as shown in Figure 1. Kinetic simulations reveal that the dominant reactions leading to knock change, depending on the pressure and temperature conditions of the unburned mixture. Under some PT conditions, EGR is highly effective at mitigating knock, but under other conditions its effectiveness is substantially reduced.

Figure 1 displays the changing effectiveness, using lines of constant ignition delay to indicate knock propensity for the different EGR levels. For modest intake pressures representing NA or lightly boosted engines (P_{in} = 0.75 to 1.25 bar), the ignition delay contours show significant separation with EGR, indicating knock propensity differences. However, for boosted engines using higher intake pressures (1.5 to 2.0 bar), the ignition delay contours show less separation, indicating very little difference in knock propensity. Thus, under boosted conditions, EGR loses effectiveness at mitigating knock.

Researchers investigated this phenomenon for three fuels that had wide variations in composition and fuel properties, including an octane sensitivity range from 1.2 to 10.7, and ethanol concentration from 0% to 30%. Experimental and computational results confirmed that the same trend was present with all fuels: EGR is effective at mitigating knock at NA or lightly boosted conditions, but loses effectiveness at higher intake pressure.

This research confirms that EGR is effective at knock mitigation for NA engines. As a result, its use at full-load can enable higher efficiency through higher compression ratio and/or advanced combustion phasing. However, there is a diminishing effectiveness at higher intake pressures that will likely prevent the same strategy from being used for boosted engines.

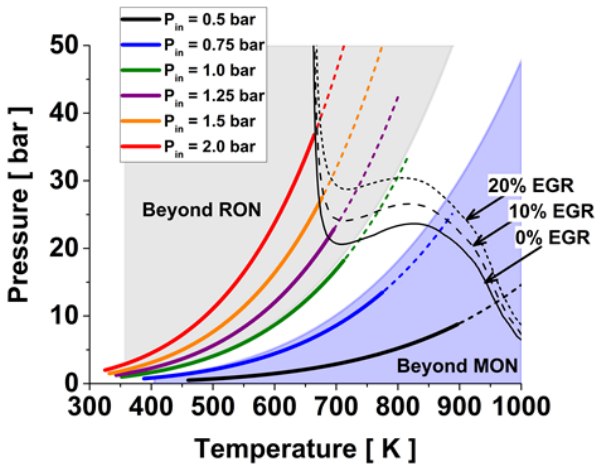

Figure 1. Pressure-temperature path of the unburned fuel-air mixture during compression for different intake manifold pressure (P_{in}). Also shown are lines of constant ignition delay (8ms) for 0%, 10%, and 20% EGR.

2017 U.S. DRIVE Highlight

Light-Duty Diesel Emissions Predicted with Computational Fluid Dynamics

High-performance computing and graphics processing unit-enabled chemistry solvers enabled refinements to kinetics, spray modeling, and mesh resolution to provide improved prediction of diesel emissions.

Oak Ridge National Laboratory, Lawrence Livermore National Laboratory, General Motors, and Convergent Science

General Motors, Oak Ridge National Laboratory (ORNL), Lawrence Livermore National Laboratory (LLNL), and Convergent Science partnered on a multi-year effort to use high-performance computing (HPC) to improve the predictive accuracy of engine simulations. Advanced modeling tools such as computational fluid dynamics have potential for designing and calibrating new engines. The need for engine simulation over the full operating space creates a tradeoff between model complexity needed for accurate predictions and computational time. The team addressed this tradeoff by using ORNL's Titan massively parallel supercomputer with LLNL's Zero-RK graphics processing unit (GPU)-enabled chemical-kinetics solver to have calculations with more predictive, physics-based sub-models and greatly reduced computational times.

The team performed simulations of 600 cases representing a multi-parameter diesel engine calibration for a wide range of engine speed, load, exhaust gas recirculation, air-fuel ratio and injection timing to evaluate the capabilities of the model. Researchers used a simplified model for conventional computing resources as the baseline. The baseline was compared to a refined model with significantly more chemical species and reactions in the combustion simulation and refined spray boundary conditions, wall treatment, and mesh size.

Figure 1 shows the difference between the measured and predicted nitrogen oxides (NO_x) and partially burned hydrocarbons (HC) emissions at 600 points in the engine's speed and load operating map. At each point, the size of the circle in the chart is proportional to the difference between the measurement and prediction using either the baseline (blue) or refined (red) model. Scaling of the circles differs in the two charts. The baseline model had larger differences versus the measured data for NO_x at mid to high loads and HC at low loads due to poor prediction of the combustion rate. The refined model improved predicted NO_x due largely to a combination of additional chemical kinetics details and refined mesh that improved gas temperature resolution. HC predictions improved with the refined model due to additional chemical kinetics details and refinements to the spray model that resulted in more accurate burn rates.

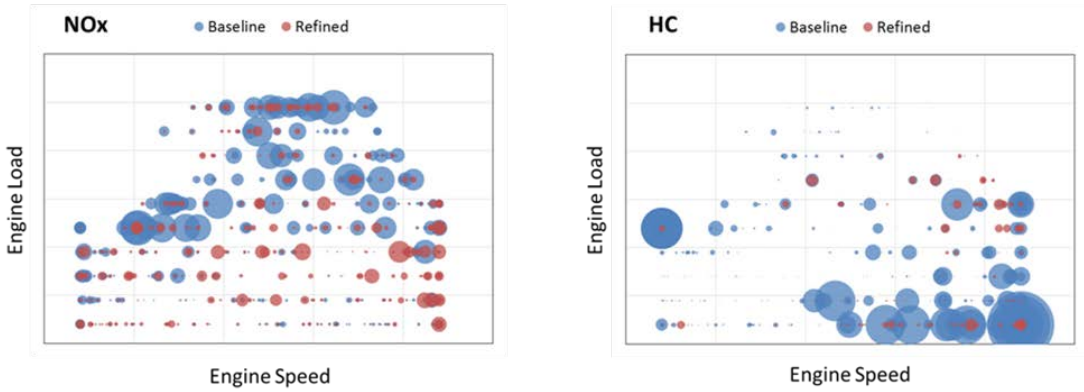

Figure 1. Difference between measured and predicted HC and NO_x emissions for the baseline and refined models at 600 engine-operating points in the engine's speed-load map. Circle size is proportional to the difference, and circle scaling differs in the two charts.

2017 U.S. DRIVE Highlight

Catalyst Demonstrates Excellent Nitrogen Oxide Reduction Performance at Low Temperature

Fundamental understanding of active catalytic center leads to the rational design of a class of catalysts with improved low-temperature nitric oxide-only performance.

Pacific Northwest National Laboratory

Lean diesel and gasoline combustion presents an attractive and necessary option for sustainable transportation by reducing carbon dioxide (CO_2) emissions and decreasing carbon footprint via maximizing fuel efficiency. However, lean combustion at lower temperatures presents unique challenges to achieving regulatory compliant emissions, including decreased temperatures for engine exhaust aftertreatment, and removing oxides of nitrogen (NO_x) under oxidizing conditions. A class of copper (Cu)-based selective catalytic reduction (SCR) catalysts built upon the small-pore, 8-ring, chabazite zeolite has proven superior to its predecessors in activity, selectivity and durability. Much of this improvement has been attributed to pore size restriction and confinement effects. Recent research by Pacific Northwest National Laboratory (PNNL) has led to improved understanding of the low-temperature rate-limiting oxidation half-cycle of the standard SCR reaction, and demonstrated a pathway towards superior SCR activity at lower temperature.

The two active catalytic centers on Cu-chabazite SCR catalysts have recently been identified, with a redox cycle mechanism established in which Cu ions cycle between Cu^{I} and Cu^{II}. The reduction half-cycle of the nitric oxide-only standard SCR reaction is reasonably well understood, but the oxidation half-cycle that is rate limiting at low temperature has been less clear. Additionally, proposals that assume redox cycling of individual isolated Cu ions do not account for the unique experimental observations at low temperature.

PNNL research has led to the discovery that the low-temperature oxidation half-cycle of the standard SCR reaction only occurs with the participation of two mobile Cu-ammonia (NH_3) complexes. Furthermore, PNNL's research has identified that the cycle is realized by the formation of a transient Cu-dimer intermediate homogeneously within the SSZ-13 pores, whose formation is rate limiting at low Cu loadings. Then, these Cu-NH_3 complexes that are stable at lower temperature dissociate at higher temperature, leaving isolated Cu ions stabilized within the zeolite lattice to support the reaction's oxidation half-cycle.

Through catalyst design to higher Cu loading, PNNL demonstrated that forming the Cu-dimer intermediate is no longer rate limiting at low temperature. This accomplishment has thereby helped to mitigate the huge entropy penalty associated with forming the Cu-dimer intermediate for reoxidizing Cu(I). As shown in Figure 1, these efforts have led to development of Cu-SCR catalysts with significant improved performance at low-temperature in comparison to current SCR catalysts.

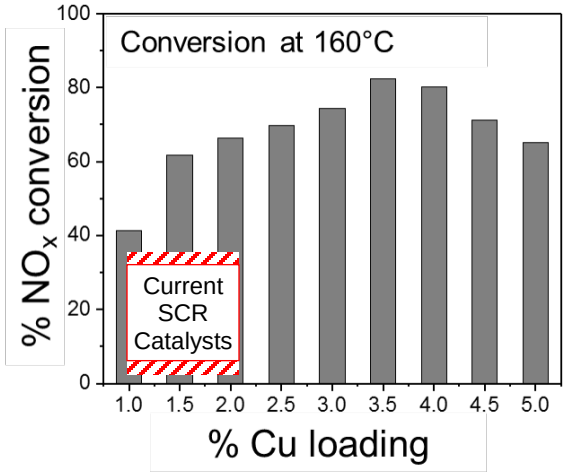

Figure 1. Steady-state NO_x conversion of candidate Cu-SCR catalysts at 100k hr^{-1} space velocity in simulated exhaust, showing optimized Cu loading to minimize the energy requirements for re-oxidizing Cu(I) in the oxidation half-cycle of the standard SCR reaction.

2017 U.S. DRIVE Highlight

High-Speed Diagnostics Probe Diesel Spray Mixing and Soot Formation Processes

Unique light sources enable unprecedented time-resolved measurements that clarify the structure and evolution of spray mixing and soot formation—providing critical data for combustion model development.

Sandia National Laboratories

Optimized fuel-air mixing is key to developing cleaner and more efficient diesel combustion. Quantitative, temporally-resolved measurements of the diesel fuel mixture field are needed for a full understanding of spray vaporization and mixing dynamics, while quantitative measurements of the soot field evolution provide insight into the coupling between mixing and pollutant formation. New light sources developed at Sandia National Laboratories have enabled unprecedented measurements that allow an accurate description of the fuel vaporization, vapor-phase mixing, and soot formation processes to be obtained.

Characterizing the fuel spray vaporization and the evolving soot field (see Figure 1) is accomplished via an extinction imaging diagnostic that relies on an R&D 100 winning pulsed light-emitting diode (LED) driver, which enables strobed illumination with ~10 nanosecond light pulses at MHz repetition rates. This high-speed diagnostic has revealed the location and timing of soot onset, the rates of soot mass formation, and the existence of a soot onset temperature limit.

A one-of-a-kind, high-power 100-kHz pulse-burst laser provides the higher photon energies necessary to quantify the fuel-air equivalence ratio (mixture fraction) field. Time-resolved images of the mixture field allow extraction of turbulent spatiotemporal correlations (structure functions), which are critical for constructing improved models applicable to the highly transient environment created by modern multiple-injection schedules. Together with the detailed measurements of soot formation and oxidation, this laser illuminates the link between mixing and soot processes and identifies critical features that combustion models must capture.

These new diagnostics expand an array of previously leveraged experimental tools, including schlieren imaging for vapor penetration and ignition characterization, excited state hydroxyl radical chemiluminescence imaging, and natural luminosity imaging. Jointly, the data provide critical information needed to formulate and validate high-fidelity models that will enable the cost-effective design of the next generation of high-efficiency, low-emission engines.

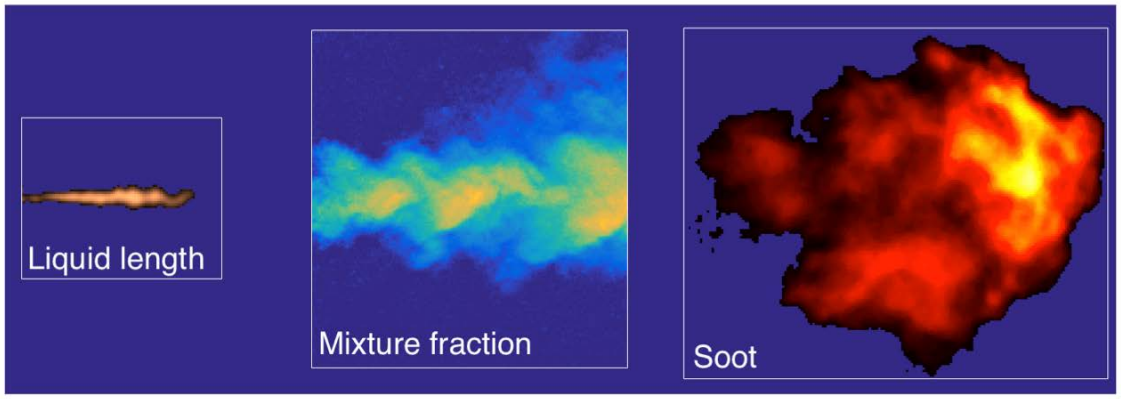

Figure 1. A collage of images demonstrating three high-speed, quantitative diagnostics. The liquid length and soot images were obtained using a Sandia-developed LED driver that generates unprecedented light intensity at high repetition rates, while the mixture fraction field used a newly developed 100-kHz pulse-burst laser. The mixture fraction and soot images correspond to the same time after start of injection (1.8 ms ASOI) for 1,500 bar n-dodecane sprays injected into a 900 K, 60 bar ambient. All images are to scale.

2017 U.S. DRIVE Highlight

Improved Understanding of Diesel Efficiency Gains with a Stepped-Lip Piston

A stepped-lip piston geometry affects turbulent flow structures and mixing, increases the rate of heat release, and improves engine efficiency.

Sandia National Laboratories

Current research at Sandia National Laboratories focuses on the in-cylinder phenomena responsible for improvements in thermal efficiency resulting from a change of piston bowl geometry in a swirl-supported diesel engine. Comparative studies with a conventional, re-entrant piston and a stepped-lip piston provide the following insights.

When the main fuel injection starts between 5 and 15 crank angle degrees after top dead center (ATDC), faster mixing controlled combustion is observed with the stepped-lip bowl. This decreases the duration of the second half of the combustion event (CA50-90, Figure 1). More work is extracted from the expansion stroke for a given amount of fuel energy, thereby increasing efficiency. Bowl geometry has a small influence on wall heat-loss, and changes to wall heat-loss have a relatively small influence on thermal efficiency. With the stepped-lip piston, faster mixing-controlled combustion is more effective at improving thermal efficiency than reduced wall heat-loss. Numerical simulation results reveal unique interactions between the fuel injection jets and the stepped-lip bowl for injections starting shortly ATDC. As the jet interacts with the step, a portion of it is deflected upward at the step. It then impinges on the cylinder head, which leads to the formation of additional recirculation zones, and spreads mixture and turbulent mixing (Figure 2). Researchers produced experimental evidence for the formation of one of these recirculation zones; its existence coincides with enhanced mixing controlled heat-release rates at intermediate injection timings (boxes in Figure 1). Because piston geometry can dramatically affect turbulent flow structure and mixing, it can directly influence engine efficiency.

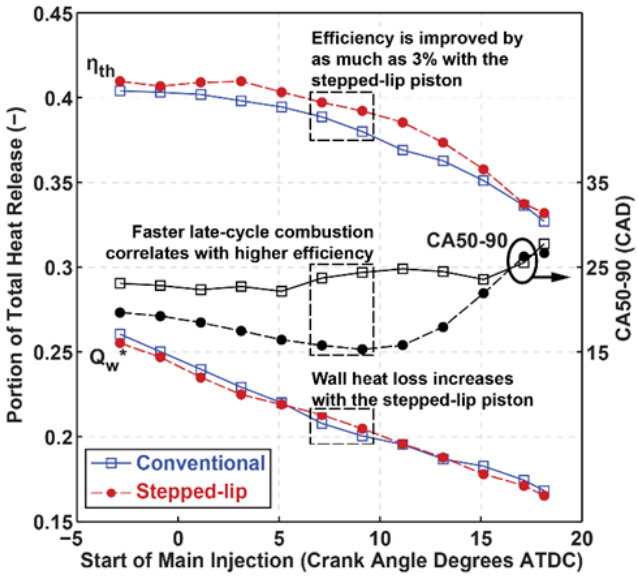

Figure 1. Piston bowl geometry may weakly influence wall heat loss, but its impact on mixing controlled heat release rates has a significant impact on thermal efficiency.

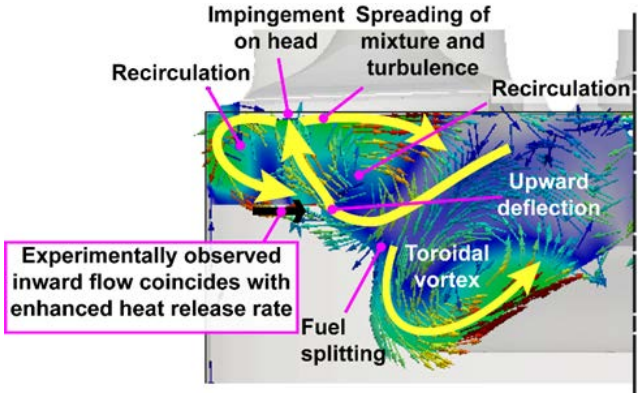

Figure 2. Spray-wall interactions with the stepped-lip bowl result in impingement on the cylinder head, recirculation, and enhanced spreading of turbulence and mixture.

2017 U.S. DRIVE Highlight

Key Physics Driving Gasoline Spray Collapse Revealed

High-speed flow measurements show that the breakdown of the central recirculation zone drives spray collapse—leading to fuel-rich mixtures, surface impingement, and particulate emissions.

Sandia National Laboratories

Gasoline direct-injection (GDI) engines face challenges with respect to cold-start and particulate number/mass emissions. Poorly mixed fuel that impinges upon the piston or cylinder liner is a source of both particulates and inefficiency. Although current multi-hole fuel injectors are designed to widely disperse and mix the fuel, experience shows that the fuel plumes interact with each other and may "collapse" into a single plume—resulting in poor mixing, over-penetration, and impingement. The phenomenon of spray collapse is not understood well and is difficult to predict using current spray modeling practices.

Researchers at Sandia National Laboratories have developed a unique, high-speed velocity diagnostic and applied it to GDI sprays (Figure 1). Planar flow velocity data are acquired at 100 kHz to capture the complex air motion during and after injection. The diagnostic reveals the fundamental fluid mechanics that initiate plume interaction and lead to spray collapse, while also providing the first quantitative dataset of this type for model development and validation.

Spray collapse, in a typical 8-hole injector, proceeds from the formation of a strong central recirculation zone between plumes shortly after the beginning of injection. This zone is indicative of an entrainment field that pulls the plumes together, causing the spray angle to depart from the designed injector drill-angle. As the plumes move toward each other, the recirculation flow breaks down (before the end of injection) and the flow eventually reverses as the plumes combine completely.

Comparison with existing computational fluid dynamic simulations shows that proper tracking of this measured velocity field is key to the success of the spray model. When the simulations accurately represent the velocity between plumes, there is better fidelity for predicting the degree of plume contact and interaction, redirecting plumes throughout time, and final collapse of all plumes.

The understanding provided by these data, and the predictive spray modeling they support, are critical for optimizing the fuel preparation process for clean, high-efficiency engines.

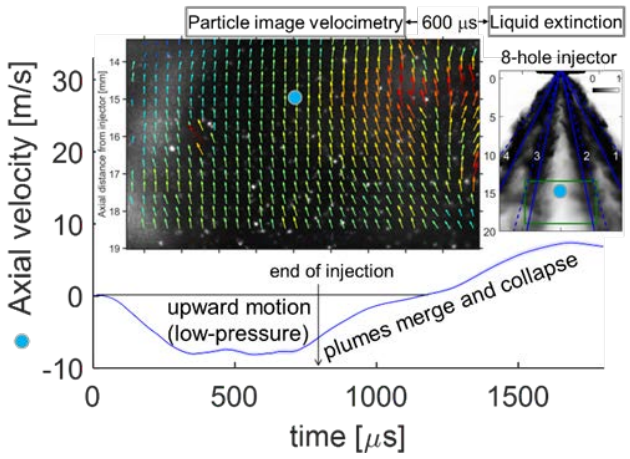

Figure 1. Left inset: Flow image at 0.6 ms after start of injection showing that a recirculation flow is setup prior to plume collapse. Right inset: Imaging of liquid plumes. The solid lines are the measured plume directions, and the dashed lines show the hole drill-angle projection. The green box shows the particle image velocimetry imaging region. Bottom: Mean velocity at the centerline, 15-mm position (blue dot).

2017 U.S. DRIVE Highlight

Ozone Addition Enhances Compression Ignition of Gasoline and Provides Combustion Timing Control

Significant reductions in required intake temperature and a wide range of timing control are achieved with parts per million levels of added ozone.

Sandia National Laboratories

Future mixed-mode gasoline engines may employ advanced compression ignition (ACI)—where combustion is initiated by compression-induced auto-ignition—at low-to-moderate loads. Such a strategy greatly improves vehicle fuel economy through reducing throttling and heat transfer losses, while maintaining low engine-out pollutant emissions. The major implementation barrier is achieving controllable auto-ignition for a range of relevant operating conditions. Proposed ACI control strategies seek to alter charge reactivity through some combination of tailored fuel-air mixing (e.g., injection strategy, charge motion, bowl geometry) and increased charge temperature (e.g., intake heaters, valve overlap). However, these solutions add cost and complexity to the vehicle.

Sandia National Laboratories has shown that intake ozone (O_3) addition is a viable way to reduce charge heating needed to control auto-ignition. The team performed research with an optically-accessible single-cylinder engine with a 13:1 compression ratio. The 50% burn angle (CA50) for a representative low-load ACI operating point is mapped in Figure 1 as a function of intake O_3 and temperature. Results show that for fixed CA50, 25 ppm of added O_3 reduces the required intake temperature by 65°C. Moreover, at fixed intake temperature, O_3 concentration variations between 0 and 35 ppm enabled robust combustion phasing control (±5°).

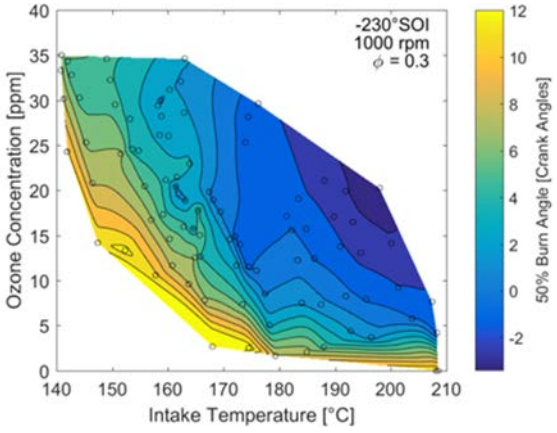

Figure 1. Map of CA50 for a range of intake temperatures and O_3 concentrations. Black circles denote experiment test points.

Researchers also performed quantitative optical measurements of in-cylinder O_3 concentration at several intake temperatures to assess complementary chemistry modeling. Figure 2 highlights the rapid thermal decomposition of O_3 near top dead center, behavior that was reasonably well-captured by the models. The modeling indicates this O_3 decomposition leads to a burst of highly-reactive atomic oxygen (O) just before auto-ignition, which rapidly abstracts fuel hydrogen to form hydroxyl radicals that alter and accelerate subsequent low-temperature ignition pathways.

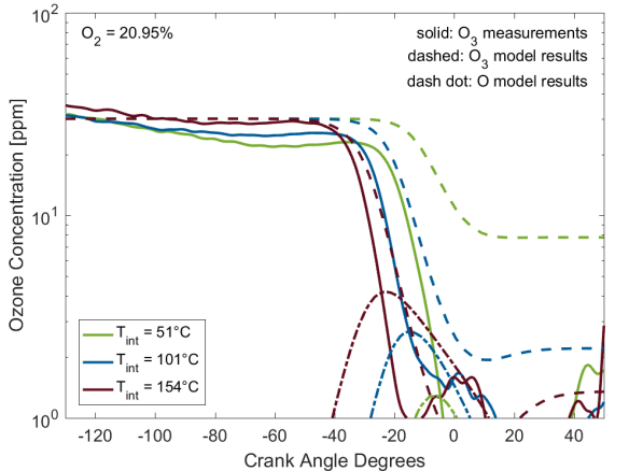

Figure 2. Quantitative in-cylinder O_3 measurements compared to complementary chemistry modeling results of O_3 and O.

In summary, O_3-enhanced ignition reduces ACI hardware requirements needed to achieve stable combustion phasing, provides a significant level of combustion timing control, and is expected to facilitate transitions from ACI to conventional spark ignition operation at higher loads.

2017 U.S. DRIVE Highlight

Transient Spark-Ignition Engine Operation Reveals Benefits of Fuels with High Octane Sensitivity

Fuels with a large difference between research and motor octane numbers provide superior knock suppression during vehicle acceleration, offering increased performance and fuel economy.

Sandia National Laboratories

Auto-ignition or "knock" in spark-ignition engines limit engine efficiency, performance, and reliability and must be avoided to ensure smooth engine operation. Knock often occurs during extended, steady operation at a high engine load, but can also be problematic under transient operation, when the vehicle is accelerating. To supplement conventional steady-state testing, researchers at Sandia National Laboratories have developed methods to test fuel knock resistance under conditions typical of vehicle acceleration.

The knock resistance of a gasoline-like fuel is measured in the research octane number (RON) and motor octane number (MON) tests. Octane sensitivity *S* is defined as the difference between RON and MON, and the octane index (OI = RON – K**S*) is thought to provide a better measure of knock resistance than RON or MON alone.

Figure 1 shows a comparison of knock-limited combustion phasing acquired with seven different fuels; lower values correspond to improved knock resistance. Under steady-state conditions (solid lines) at an intake pressure of 100 kPa, the RON 98 fuels have the same knock limit regardless of *S*—indicating that the in-cylinder conditions are comparable to the conditions of the RON test (K=0).

To simulate transient conditions that mimic vehicle acceleration, the engine was fired for 20 cycles, followed by 80 motored cycles, with the 20/80 sequence repeating until quasi steady-state conditions were established. At that point, with the spark timing adjusted to render a moderate knock level, 1,000 cycles were acquired and the average knock limit (KL-CA50) computed. The relatively cool combustion chamber surfaces established by the alternate fired/motored engine operation, in combination with a high load, result in conditions that are well beyond the RON octane test, as reflected by a negative K value. Figure 1 shows that for these cooler transient conditions (dashed lines) all fuels are less knock limited. To first order, the anti-knock quality of the fuels was found to be consistent with their RON and *S*. Accordingly, fuels with a higher octane sensitivity benefit the most from the cooler state of the engine.

For boosted operation with P_{in} greater than 100 kPa, the best knock suppression is observed for the two butanol blends, which modestly outperformed fuels with equal or higher sensitivity. This observation warrants further examinations of advanced fuel blends with high octane sensitivity. It is also noteworthy that under transient conditions, the RON 92 fuel outperforms the Alkylate fuel, which has a higher RON of 98. This highlights the importance of high octane sensitivity.

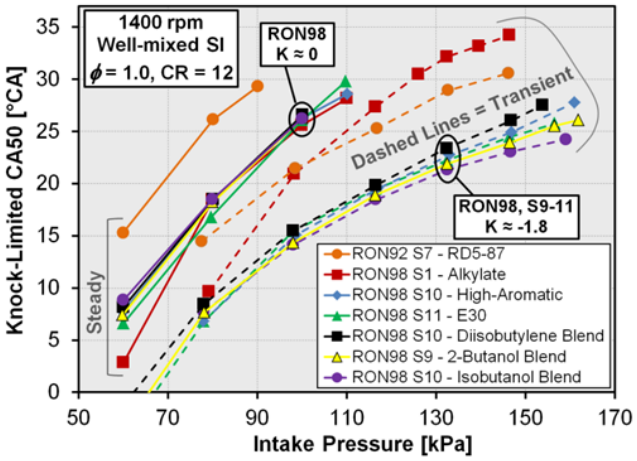

Figure 1. Knock-limited combustion phasing (CA50) as a function of intake pressure, both for steady-state and load-transient operation. Lower values indicate higher knock resistance.

Electrical and Electronics

2017 U.S. DRIVE Highlight

Cost-Effective Fabrication of High-Temperature Ceramic Capacitors for Electric Vehicle Inverters

New fabrication technology can make low-cost ceramic capacitors with high dielectric constants and breakdown strength, enabling lighter and smaller power electronics for vehicle applications.

Argonne National Laboratory

Essential components of power electronics, capacitors carry out a host of functions necessary in vehicle applications. Ceramic capacitors have the potential for significant volume reduction—up to 30% smaller than the polymer-based capacitors currently used in electric vehicles (EVs). Ceramics offer high dielectric constants and breakdown fields and, therefore, high energy densities. They also can tolerate high temperatures, enabling them to carry high ripple currents, even at elevated temperatures.

Previous research has shown that lead lanthanum zirconate titanate (PLZT) film capacitors have desired performance characteristics, but fabrication methods are impractical. To overcome this drawback, a high-rate, room-temperature aerosol deposition (AD) process has been developed that can produce large-area dense PLZT films. This process accelerates PLZT particles toward a substrate, and the particles consolidate upon impact—without additional heating of the substrate. Without the need for this calefaction, the substrate can be a flexible material such as polymer, plastic, thin metal foil, glass, etc. Using pliable substrates enables production of PLZT-based capacitors in a wound configuration, similar to the currently used polymer-based capacitors with benign failure features.

U.S. DRIVE partner Sigma Technologies successfully demonstrated the production of wound high-temperature ceramic capacitors with benign failure feature using metallization similar to wound polymer capacitors (Figure 1). Using a Sigma Technologies prototype deposition system, researchers fabricated PLZT tapes up to 12” long on metallized polyimide films. These films were wound, arc-sprayed, and made into capacitors. Further scale-up of the process for material deposition and capacitor development at a vehicle-scale prototype is needed before this technology completes the transition to vehicle applications.

Figure 1. Long-length PLZT films were wound around a core with a separator layer of polyimide film, demonstrating the potential to make wound high-temperature ceramic capacitors.

The capacitors fabricated possess excellent dielectric properties that are promising for high-power applications such as those needed in EVs. Furthermore, using aluminum electrodes and polymer films reduces the cost of the capacitor, and the rolled/stacked and embedded capacitor construction approach significantly reduces the capacitor carbon footprint. These capacitors offer improved device performance, greater design flexibility, and economic advantages for commercialization. This technology will achieve the desired high degree of packaging volumetric efficiency with less weight. In addition, the device has fewer and smaller interconnections, which improves its reliability.

2017 U.S. DRIVE Highlight

Increased Accuracy of Motor Material Parameters Enables Reduced Design Cost and Time

National Renewable Energy Laboratory model for stator-to-case thermal resistance enables increased accuracy and reduces design iterations for developing power-dense electric motors.

National Renewable Energy Laboratory

For motors cooled through the case and the surrounding cooling jacket, the thermal contact resistance between the electric motor stator and the cooling jacket is a significant factor in overall performance. The National Renewable Energy Laboratory (NREL), in collaboration with UQM Technologies, developed and demonstrated a physics-based model for stator-to-case thermal resistance (Figure 1a) that improves the accuracy of data available to electric motor designers, helping them accurately estimate the stator-to-case thermal contact resistance for a range of electric motors. Increasing the precision of key motor design parameter information translates into fewer design iterations—and hence a more cost-efficient and accurate design process—for developing power-dense electric motors.

The stator-to-case interface is typically an interference fit subject to compressive pressure exceeding 5 MPa. Existing thermal contact resistance models, when applied to the interface in an interference fit cooling jacket, result in a wide range of estimated thermal contact resistance ranging from 149 mm^2 K/W to 1,400 mm^2 K/W. In electric motor thermal design, this wide range results in a temperature gradient across the interface gap that can vary by a factor of seven.

Using NREL's high-pressure thermal transmittance setup, researchers experimentally investigated the contact interface thermal resistance between the stator steel laminations and the aluminum housing for pressures ranging between 5.5 and 9.6 MPa, representing an interference fit between the stator and the case for multiple materials. The model included both solid and fluid (air) interface components to calculate thermal contact resistance. The solid-to-solid contact conductance model accounts for the surface roughness of the two contacting surfaces (Figures 1b and 1c), the applied pressure, and the material hardness. The solid-to-fluid conductance model incorporates the thermal conductivity of the interstitial gas, the contact pressure, and the material hardness. The comparison of modeling results and experimental data for one material is shown in Figure 1d. The error bars for the experimental data represent the 95% confidence interval, incorporating random and systematic experimental uncertainties.

A manuscript summarizing the results of this work has been accepted for publication in a journal.

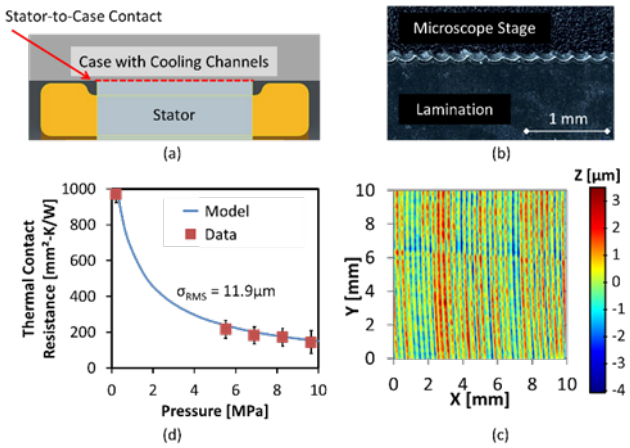

Figure 1. (a) Cross-section view highlighting a stator-to-case interface. (b) edge view of one sample lamination showing a serrated edge. (c) 10 mm-square sample area surface profile of the contact plate representing a cooling jacket machined surface. (d) comparison of results from the model and experimental data.

2017 U.S. DRIVE Highlight

NREL Collaborates with Industry Partner to Develop Power-Dense Two-Phase-Cooled Inverter Design

Research shows potential design of two-phase evaporator and condenser to enable flexible and modular heavy-duty inverter.

National Renewable Energy Laboratory

Scalable and modular power electronics systems such as inverters must be compact and power-dense to enable vehicular applications, and require advanced cooling strategies that reliably and effectively manage heat from power electronics components. Prior U.S. Department of Energy-supported research at the National Renewable Energy Laboratory (NREL) focused on developing and characterizing passive two-phase cooling technologies (Figure 1) for power electronics applications. The self-contained passive two-phase system enables using high-density power electronics in applications without using conventional water-ethylene glycol (WEG) liquid cooling. The proposed phase-change cooling system eliminates hoses, pumps, and WEG coolant leaks. Experiments demonstrated improvements in heat transfer for two-phase cooling with respect to conventional WEG liquid cooling, as shown in Table 1 for systems of similar volume.

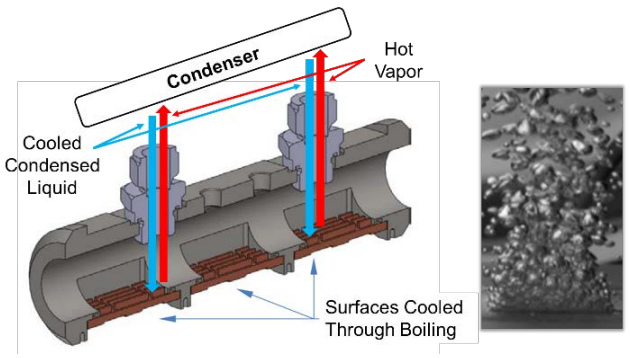

Figure 1. Left: Cross-sectional view of the evaporator vessel showing flow of two-phase fluid, with vapor rising from the surface being cooled to a condenser and the cooled fluid returning back to the evaporator. Right: Image of two-phase heat transfer with vapor bubbles generated on the surface to be cooled.

As a result of this research, NREL and John Deere Electronic Solutions (JDES) signed a cooperative research and development agreement to support the transfer, development, and demonstration of this technology for heavy-duty power electronics applications. The collaboration between NREL and JDES focused on two key application challenges, with NREL providing two-phase thermal and flow analysis though finite element analysis and computational fluid dynamics (CFD) simulations. The first challenge was to develop a compact passive pool boiling evaporator that would have sufficient safety margins for operating below the critical heat flux limit within temperature and pressure constraints. The second challenge was developing a modular integrated condenser meeting application research constraints. Modeling and analysis efforts focused on these two challenges to demonstrate concept viability. The preliminary design enables an air-cooled system targeted for 70°C ambient air while maintaining peak device temperatures below 150°C. The air-cooled inverter with the integrated passive two-phase evaporator is expected to achieve a power density exceeding 13 kW/L.

Weight reduction	Heat dissipation increase
41%	139%

Table 1. Percent reduction in weight and percent increase in heat dissipation using a passive two-phase cooling system.

With the initial proof-of-concept design complete, research is continuing into the next project phase. Enhanced models for two-phase heat transfer are being developed at NREL (integrated into commercial CFD software) to further optimize the design. While modeling continues, proof-of-concept hardware is being fabricated for concept validation experiments.

2017 U.S. DRIVE Highlight

High-Power Density Motor without Permanent Magnets

Motors without permanent magnets are critical to achieving low-cost, high-power density electric traction drives.

Oak Ridge National Laboratory

Most electric vehicle and hybrid electric vehicle motors use permanent magnets with heavy rare-earth (HRE) materials such as neodymium and dysprosium because they facilitate achieving high power densities, specific powers, and efficiencies. However, significant market volatility has been associated with HRE materials, including a 40-fold price increase in dysprosium within a year. Developing viable alternatives to HRE-based machines is critical to increasing the stakeholder confidence that facilitates mass production. Achieving competitive performance and efficiency with alternative motor technologies having comparable mass, volume, voltage, and other key metrics requires an advanced multidisciplinary research approach. Therefore, this project involves high-accuracy modeling and comprehensive nonlinear computational optimization of geometric features and winding parameters.

The project developed a general nonlinear direct quadrature modeling method that quickly and accurately evaluates simulated motor characteristics under voltage and current constraints. While considering electromagnetic, mechanical, and thermal performance, Oak Ridge National Laboratory (ORNL) optimized geometric parameters and winding arrangements and fabricated and tested the design shown in Figure 1.

Figure 1. ORNL's synchronous reluctance prototype motor lamination (left) and motor assembly (right).

The unique synchronous reluctance motor design's performance greatly improved, thanks to using reconfigurable winding arrangements; simulated peak power reached over 100 kW at 9,500 RPM, and researchers measured a maximum power of 84 kW at 10,000 RPM. Table 1 summarizes key simulated and measured performance metrics.

Speed (RPM)	Peak Power (kW)	Power Density (kW/L)	Specific Power (kW/kg)
DOE Target	55	5.7	1.6
9,500 (simulated)	102	7.7	2.8
4,000 (measured)	64	4.8	1.7
10,000 (measured)	84	6.3	2.3

Table 1. Simulated and measured performance data.

U.S. Department of Energy targets for power density and specific power are 5.7 kW/L and 1.6 kW/kg, respectively, and the synchronous reluctance motor meets these. Figure 2 shows measured performance data and efficiency contours. A significant portion of the operation range reaches above 90% efficiency. Overall, this motor is a viable candidate for electric drive motors but requires further materials and design research to increase operational efficiency.

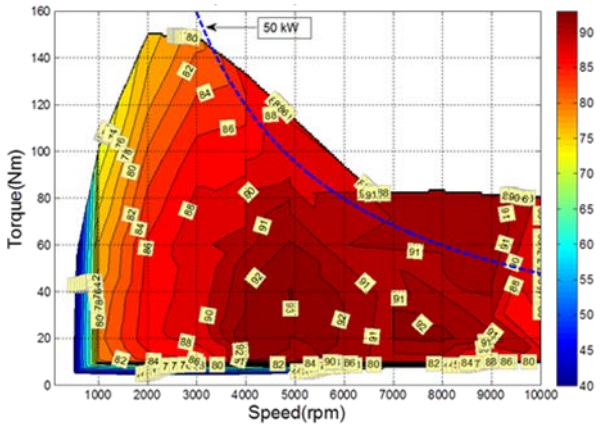

Figure 2. Performance and efficiency data from dynamometer testing of ORNL's prototype motor with no magnets.

Low-Inductance Power Module Design

A low inductance value of 5.2 nH per device was achieved for high-switching-frequency (greater than 50 kHz) operation of a 30 kW wide bandgap boost converter.

Oak Ridge National Laboratory

Lowering the average parasitic inductance per device for boost converter modules allows for higher switching frequency and speed operation, which helps increase the power density of the drivetrain's overall power conversion stage. Successful efforts to lower power module inductance will help achieve the U.S. Department of Energy's 2020 power density targets.

An Oak Ridge National Laboratory research team has achieved a low inductance value of 5.2 nH for a 30 kW boost converter module with six devices in parallel. This result corresponds to a roughly 66% reduction compared to a commercial silicon carbide (SiC) metal–oxide semiconductor field-effect transistor (MOSFET) power module. The researchers use a p-cell, n-cell packaging concept to attain the low power loop parasitic inductance.

In the power module (Figure 1), dedicated Kelvin drain and source pins are designed for accurate measurement of the real voltages across the devices during switching transients. A three-dimensional printed housing presses the direct bonded copper (DBC) substrates in close contact with the baseplate. Thermal grease is used between the bottom of the DBC and the top of the baseplate. All the gate signals and voltage sensing signals are connected to the gate drive board, which is mounted on top of the module. The fabrication procedures include several steps: 1) die-attach and pin-attach (gate, source, and voltage sensing pins); 2) die interconnection using 5-mil wire bonds; 3) power terminal attach and house attach; and 4) encapsulation to protect the die and wire bonds from mechanical and chemical damage.

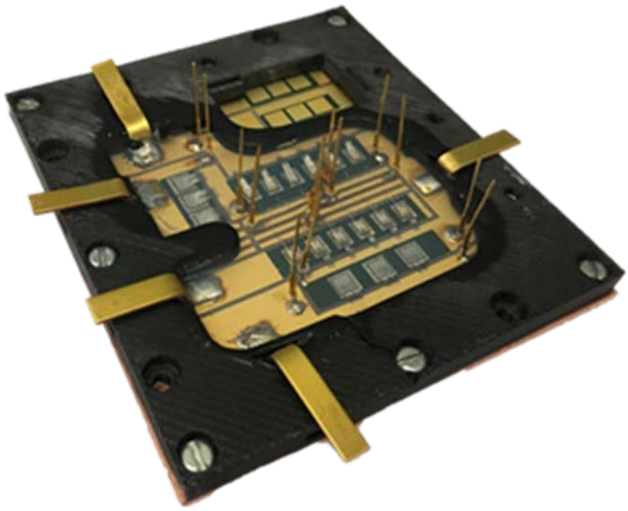

Figure 1. Fabricated SiC trench MOSFET module.

The parasitic inductance of the power module is extracted experimentally. The voltage across the decoupling capacitance is compared with the real drain-to-source voltage across devices, and the parasitic inductance values are derived from the voltage difference and drain current slew rate measured from coaxial shunt. The researchers compared the reduced inductance value with simulation results, finding an excellent match.

Although this concept was designed for boost converter modules, it can also be used in other power modules, allowing higher frequency operation at high efficiency.

2017 U.S. DRIVE Highlight

Multilayered Film Capacitors for Advanced Electric Vehicle Traction Drives

New film has demonstrated an improved dielectric constant and breakdown strength as compared to currently used polypropylene films.

PolymerPlus LLC

Biaxially oriented polypropylene (BOPP) film capacitors are the most suitable technology for high-voltage, high-temperature, and high-ripple-current power electronics systems in electric vehicles (EVs). These capacitors, however, can occupy one-fourth to one-third of the power electronic unit volume and have a 50% voltage derating above 85°C because, at high temperatures, their breakdown strength and lifetime deteriorate drastically. A new dielectric material system for capacitors—one that allows for increased temperature use and reduced size—would enable many EV-related applications. Multilayer dielectric film developed by PolymerPlus, with support from partner organizations, has demonstrated an improved dielectric constant and breakdown strength as compared to BOPP films (Table 1).

Capacitor Properties	Commercial BOPP	Multilayer Film
Temperature	<105°C	150°C
Loss	<1%	<1%
Dielectric constant	2.25 (1 kHz)	4 (1 kHz)
Breakdown strength	800 MV/m	>1,100 MV/m

Table 1. Dielectric performance summary of multilayer dielectric film.

The PolymerPlus project team developed several film formulations and evaluated their dielectric performance. The team processed and metallized three film rolls, with a total length of 28,000 square feet. Down-selection of the more promising products was based on their potential for production scale-up. Because this technology uses commercial polymers, the trial fabrications of film rolls successfully demonstrated a scalable production process for capacitor manufacture.

The team then successfully processed 12,000 square feet of the selected multilayer film in 8 µm and 4.3 µm thicknesses, determining that the 8 µm film allowed for better metallization and capacitor winding.

The project culminated in development of prototype 600 µF capacitors, representing the typical capacitor sizes needed for EV traction drive systems (Figure 1).

Further development and analysis are required to gain a full understanding of multilayer film behavior in these large-scale capacitor parts, and vehicle application-specific engineering or development has yet to be performed on these parts.

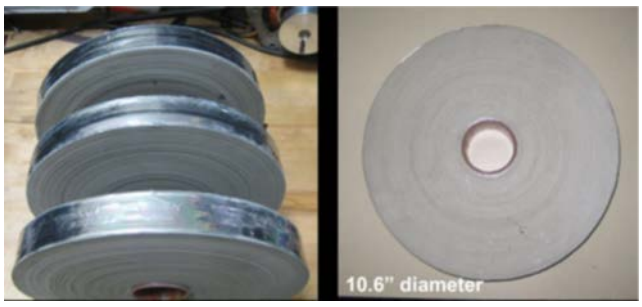

Figure 1. 600 µF capacitor prototypes using multilayered dielectric film.

Electrochemical Energy Storage

2017 U.S. DRIVE Highlight

Low-Cost Semi-Solid Cell for Electric Vehicle Applications

24M Technologies has developed a breakthrough manufacturing process that leverages proven and emerging chemistries to produce lithium (Li)-ion batteries with lower cost and inactive materials content than any existing Li-ion cell.

24M Technologies, Inc., and the U.S. Advanced Battery Consortium

In the electric vehicle industry, the cost of battery materials in the cell is $50 to $75/kWh, yet total cell costs exceed $200/kWh due to high manufacturing costs. 24M has simplified the lithium (Li)-ion manufacturing process to create a cell that promises to be significantly lower in cost than traditional Li-ion cells. Additionally, conventional Li-ion cells contain many components that do not store energy. These inactive materials take up weight and space in the cell and add to the cost. 24M's unique manufacturing process enables thicker electrodes with more energy-producing materials and less inactive material, further reducing cost.

In a conventional Li-ion cell manufacturing line, materials to provide and store Li (active materials) are mixed with solvents, coated onto conductive metal foils, and then dried and calendared to produce electrodes. These drying lines are energy intensive, time consuming, and take up a lot of space. Electrolyte is then injected in an additional process step. In contrast, 24M mixes the electrolyte with the active materials before coating and thereby eliminates the drying, calendaring, and subsequent electrolyte injection steps, making the manufacturing process much simpler and less expensive (Figure 1). In addition, the electrode thickness can be increased, reducing the number of layers and lowering inactive material content. Batteries using 24M's cells have been developed previously for grid storage applications, which are less sensitive to size and weight than automotive applications. 24M is now increasing battery energy and power density while maintaining much lower manufacturing and material costs.

During the past year, 24M has screened dozens of materials and incorporated those that show the greatest promise of producing a reliable and high performing battery into the manufacturing process. By using higher energy materials, 24M has increased the energy density of larger batteries by more than 20%, and demonstrated, at a small scale, the capability to increase the energy density by more than 60%. Meanwhile, 24M has improved the life of its EV cells by more than 5x. 24M will continue to develop technology to provide batteries equivalent in performance to conventionally made cells, but with much lower material and manufacturing costs.

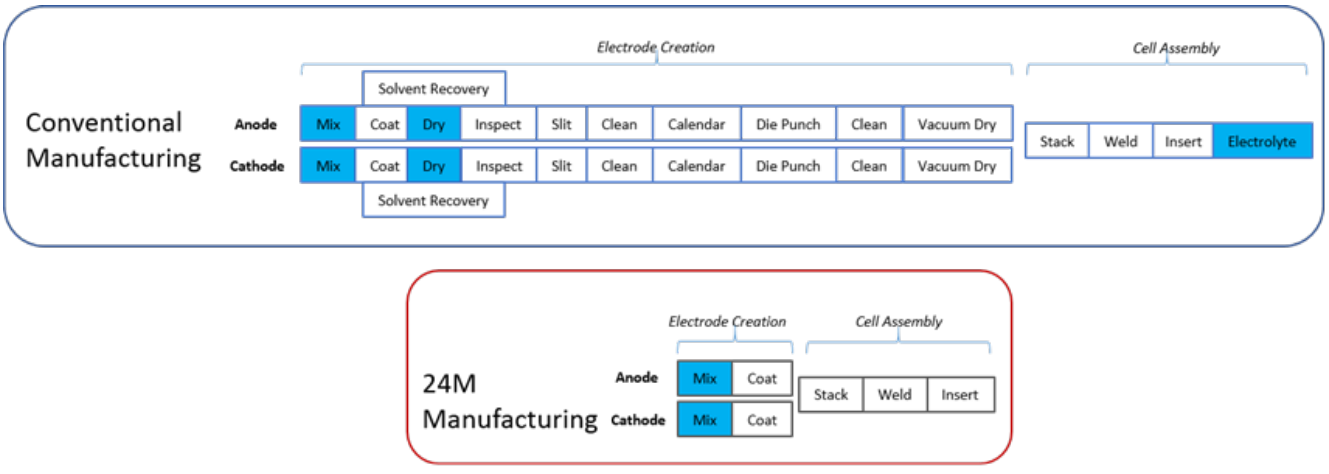

Figure 1. Using a single liquid as the mixing solvent and electrolyte, 24M's semi-solid technology reduces process complexity and cost.

2017 U.S. DRIVE Highlight

Cathode Materials with Component Concentration Gradient Structures Improve Performance

Gradient cathodes prepared using a scalable manufacturing process exhibit 20% improved capacity retention and 35% suppressed heat generation, showing a substantial breakthrough for use in electric vehicles.

Argonne National Laboratory

New active battery materials are often synthesized at the bench scale but in gram quantities with processes that are not scalable to high-volume production. To produce these materials with manufacturing-ready processes in sufficient quantity for both fundamental research and industrial commercialization, process R&D and composition optimization is needed.

Typical nickel (Ni)-rich manganese cobalt (NMC(xyz)) cathode materials offer high capacities, but suffer from rapid capacity fade and thermal instability when cycled at high voltages. To address these issues, researchers synthesized cathode materials with concentration gradient structures from high-capacity Ni-rich cores and a thermally stable manganese-rich particle surface. The goal is to produce a capacity of more than 200 mAh/g together with improved thermal stability.

Researchers selected NMC90/5/5 as the particle core composition and NMC333 as a particle surface composition (the average overall composition is NMC811). The team prepared two types of gradient materials, 811 core-gradient and 811 core-shell (Figure 1a and 1b). Figure 1c is a performance comparison of 811 core-gradient, core-shell, and commercial NMC811 cathodes. First cycle efficiency, average working voltage, and initial discharge capacity are all similar but 811 core-gradient and core-shell show 20% improved capacity retention, higher thermal decomposition onset temperature, and 35% suppressed heat generation compared with the commercial NMC811, as shown in Figure 1d.

These results demonstrate that the gradient particle structure is a practical and effective approach to stabilizing high-capacity Ni-rich NMC cathode materials, which show significant promise for use in electric vehicles.

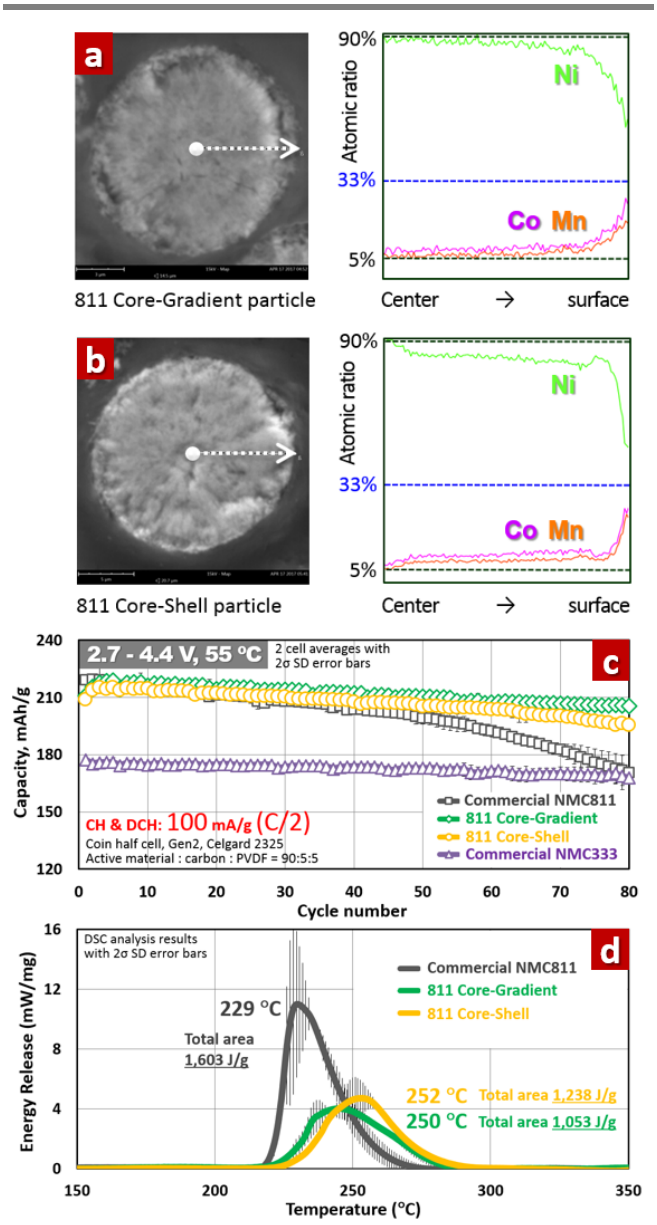

Figure 1. (a) Cross-sectional elemental mapping of the prepared 811 core-gradient cathode. (b) Cross-sectional elemental mapping of the prepared 811 core-shell cathode. (c) Comparison of electrochemical performance. (d) Thermal stability comparison.

2017 U.S. DRIVE Highlight

Oxidatively Stable Fluorinated Sulfone Electrolytes

Fluorinated sulfones with an α-trifluoromethyl group exhibit enhanced oxidation stability, reduced viscosity, and superior separator wettability as compared to their non-fluorinated counterparts. The improved performance in high-voltage cells makes it a promising candidate for next-generation high-voltage high-energy lithium-ion cells for electric vehicles.

Argonne National Laboratory

The conventional lithium (Li)-ion electrolyte is composed of 1.0-1.5 M lithium hexafluorophosphate ($LiPF_6$) dissolved in ethylene carbonate (EC), dimethyl carbonate, diethyl carbonate, and/or ethyl methyl carbonate (EMC). Designed for 4 volt (V) application, this electrolyte decomposes at potentials above 4.5 V. Therefore, the development of new and stable electrolytes for high voltage Li-ion batteries is a priority.

Aliphatic sulfones have long been studied as promising electrolytes for high-voltage Li-ion cells. Angell and Xu demonstrated good voltage stability of sulfones including dimethyl sulfone, ethyl methyl sulfone, and tetramethylene sulfone. However, these sulfones suffer from high viscosity, low conductivity, poor wettability of electrode and separator, and poor compatibility with graphitic anodes, making them unsuitable for high voltage Li-ion chemistries.

Scientists at Argonne National Laboratory have synthesized a new class of fluorinated sulfone-based electrolytes (Figure 1a). Difluoroethylene carbonate (DFEC) mixed with trifluoromethyl ethyl sulfone (FMES) and trilfluoromethyl propyl sulfone (FMPS) exhibit enhanced oxidation stability as evidenced from the capacity retention (Figure 1b) and coulombic efficiency (Figure 1c) in a $LiNi_{0.5}Mn_{0.3}Co_{0.2}O_2$ (NMC532)/graphite cell cycled at 4.6 V. These electrolytes also exhibit reduced viscosity and good separator wettability (both similar to that of the Gen 2 electrolyte (EC:EMC (3:7 by wt.) + 1.2M $LiPF_6$) and good compatibility with graphite anodes. These improved physical and electrochemical properties make it a promising high voltage electrolyte for next generation Li-ion cells.

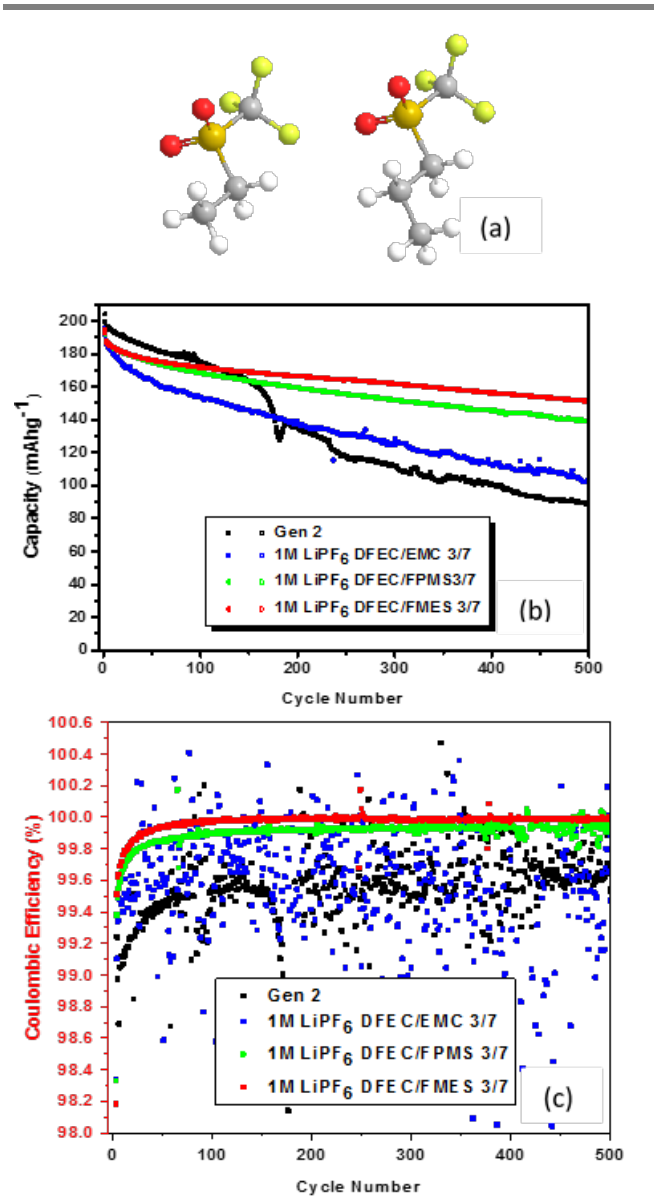

Figure 1. (a) Molecular structure of FMES and FPMS. (b) Capacity retention and (c) Coulombic efficiency of NMC532/graphite full cells cycled with 1.0 M $LiPF_6$ DFEC/FMES, 1.0 M $LiPF_6$ DFEC/FPMS, 1.0 M $LiPF_6$ DFEC/EMC, and Gen 2 electrolyte. (C/10 for 2-cycle formation and C/3 for 100 for cycling with 3.0-4.6 V cut-off voltage.)

2017 U.S. DRIVE Highlight

Self-Forming Artificial Solid Electrolyte Interphase to Protect Lithium-Metal Electrodes

This project has developed and demonstrated a simplified approach to form passivation coatings which effectively stabilize the cycle performance of lithium-metal electrodes for electric vehicle applications.

General Motors

Lithium (Li)-metal based batteries, including Li-sulfur and solid-state batteries, are among the most promising candidates of high energy density batteries. However, Li undergoes large volume changes during cycling, leading to coupled mechanical/chemical degradation at multiple length scales, including the formation of mossy structures and dendrite growth. Different strategies, such as adding electrolyte additives and applying protective coatings, have been explored to enhance the cycle efficiency of Li metal electrodes.

Researchers have found that adding fluoroethylene carbonate (FEC) into the electrolyte can improve the cycle stability by forming Li-fluoride (LiF) and a polymeric matrix as part of the solid electrolyte interphase (SEI). However, FEC is gradually consumed during the cycling process. In addition, gas generation from the reaction between FEC and Li-metal may affect battery abuse tolerance.

Researchers at General Motors Global R&D center have developed a physical vapor deposition process to coat Li-metal electrodes with fluorinated nanocomposite coatings where nano-sized LiF crystals were embedded in a carbonaceous polymer matrix, Figure 1. This self-forming nanocomposite coating effectively isolates Li-metal from the electrolyte. The flexibility of the coating makes it easy to accommodate the volume changes of the Li-metal electrode. The high conductivity of the coating leads to more uniform current distribution to encourage homogenous Li plating and stripping, thus inhibiting the formation of dendrites. The protected Li-metal electrodes, combined with high concentration salt electrolyte developed at Pacific Northwest National Laboratory, show improved cycle stability in symmetrical (Li-metal anode against Li-metal anode) cells as evidenced by the stable and low voltage during cycling, shown in Figure 2. This plot shows the large voltage variation during cycling with a standard electrolyte, which is caused by rapid impedance growth related to continuous SEI growth. The high salt concentration/coated Li metal cell does not demonstrate such voltage variation and is thus more stable during cycling. Researchers will conduct further validation studies in pouch cells using high-energy nickel-manganese-cobalt oxide or sulfur cathodes.

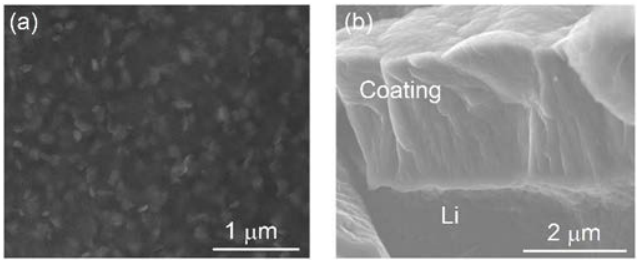

Figure 1. (a) Self-forming nanocomposite has a unique nanostructure where LiF nanocrystals embedded in polymeric matrix. (b)The cross-section image showing the coating is dense and has good adhesion to Li-metal.

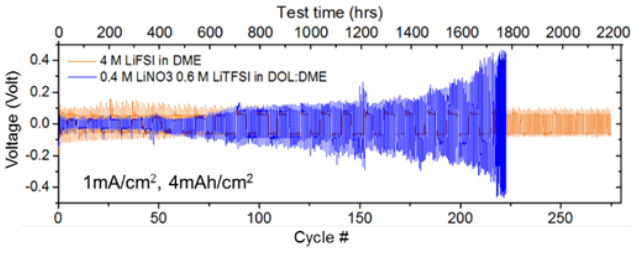

Figure 2. The combination of the protective coating with high concentration LiFSi salt in dimethoxyethane solvent enables (orange line) long-term cycle stability.

2017 U.S. DRIVE Highlight

Technical Assessment for Extreme Fast-Charging of Electric Vehicles

A combined analysis investigating the technical challenges limiting extreme fast-charging of electric vehicles includes impacts to battery performance, battery thermal management, vehicle design, and infrastructure, and economic considerations to aid development of technical targets and research and development plans.

Idaho National Laboratory, Argonne National Laboratory, and National Renewable Energy Laboratory

Extreme fast-charging (XFC), which is charging an electric vehicle (EV) at up to 400 kW, may increase the utility of an EV. Figure 1 shows how utilizing fast-charging at 50 kW for 1% to 5% of all charges correlates with a nearly 25% increase in annual vehicle miles traveled (VMT). Automotive companies, battery manufacturers, codes and standards bodies, charger manufacturers, network operators, and utility suppliers can be impacted by the use of XFC. This multi-lab project team engaged with industry to identify technical challenges and developed a report[1] outlining the limiting factors for XFC implementation in EVs. The XFC assessment focused on four pillars: batteries, vehicles, infrastructure, and economic considerations.

Battery cost is often cited as a barrier to EV adoption. XFC using current cell technology would increase the cost of a cell by more than 90% (Table 1), with anode thickness the primary cost driver. Anode thickness must be decreased to enable XFC to reduce the likelihood of lithium (Li) plating. Within cells, a bulk of the needed research centers around mitigating the onset of Li plating and minimizing heat generation, which lead to cell degradation and safety concerns. R&D into the impact of XFC on battery life (beyond Li plating issues) is also needed.

Higher voltage batteries, up to 1,000 volt (V) versus a conventional EV's 400 V systems, might enable XFC capability but would also require additional research in the electrical architecture and power electronics that support the electric drive system.

In infrastructure, XFC using a cord and plug will require research in thermal management of the charger power electronics and charge cable. For wireless charging technologies, electromagnetic field shaping and shielding require R&D. XFC's intermittent demand for electricity could pose challenges to the electric grid's stability.

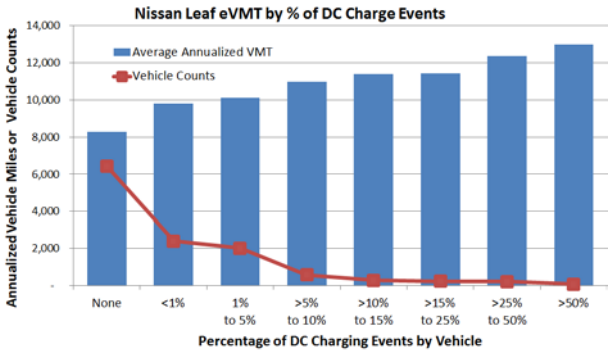

Figure 1. California Air Resource Board analysis shows increased yearly VMT when using 50 kW fast-charging. Compared with a vehicle that never fast-charged, nearly 25% increase in VMT was realized when 1% to 5% of total annual charging events were fast charges [McCarthy, Michael, 2017, "California ZEV Policy Update," SAE 2017 Government/Industry Meeting, SAE, January 25, 2017 Washington, DC, conference presentation].

Charging Time, ΔSOC=80%, minute	**8**	**10**	**23**	**47**	**53**	**61**
Charging Time, ΔSOC=60%, minute	5	7	15	30	34	39
Charger Power Needed, kW	601	461	199	100	88	77
Anode Thickness, μm	**14**	**19**	**43**	**87**	**98**	**103**
Heat Generated during Charge, kWh per pack	2.35	2.20	1.89	1.77	1.75	1.45
Post-Charge Cell Temperature (ΔSOC=80%), degrees C	22.4	24.4	25.9	26.4	26.4	19.5
Cell Mass, kg	2.75	2.40	1.74	1.49	1.46	1.45
Cell Cost to Original Equipment Manufacturer, $ per kWh	**$229**	**$196**	**$132**	**$107**	**$104**	**$103**
Cost Difference, $ per kWh	$126	$93	$30	$4	$1	$0

Table 1. BatPaC simulation comparing the effects of charging time on the required anode thickness, heat generation in the cell, cell cost, and incremental cost of charging faster than 60 minutes.

[1] Howell, et al, *Enabling Extreme Fast Charging, A Technology Gap Assessment*, https://energy.gov/eere/vehicles/downloads/enabling-extreme-fast-charging-technology-gap-assessment.

2017 U.S. DRIVE Highlight

Understanding Oxygen Redox Processes in High-Capacity Lithium-Ion Cathode Materials

Comparing two high-energy cathodes sheds light on complex oxygen redox processes that contribute to their high energy and might aid in the search for higher-energy, more-stable cathode materials.

Lawrence Berkeley National Laboratory

Lithium (Li), manganese (Mn)-rich layered oxides demonstrate a high capacity (greater than 250 mAh/g), far above the theoretical capacity originating solely from nickel (Ni) and cobalt redox (i.e., 127 mAh/g for Ni redox in $Li_{1.2}Ni_{0.2}Mn_{0.6}O_2$). Lattice oxygen (O) is believed to compensate for additional charge beyond transition metal (TM) redox. Combining TM redox with O redox has attracted significant attention because it presents a new and exciting direction for high-capacity Li-ion cathodes. However, the concept of O redox as the origin of improved cathode materials is quite new. Fundamental understanding of these redox processes is critical to proposing effective material design strategies to develop novel materials that harness active O redox and that enable further overall energy density gains from the cathode material perspective.

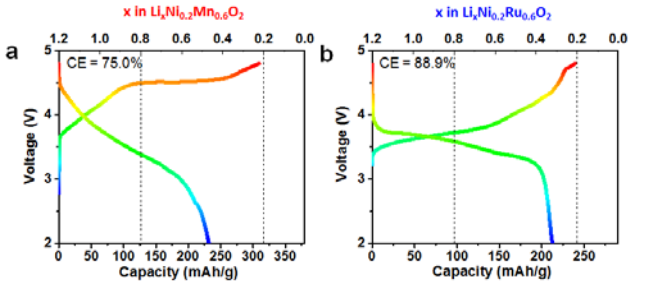

Figure 1. First charge-discharge characteristics of $Li_{1.2}Ni_{0.2}TM_{0.6}O_2$. (a) TM = Mn, (b) TM = Ru.

We probe the O redox processes in Li-rich layered oxides from a material perspective via exploration of Mn and ruthenium (Ru). As shown in Figure 1, both Li-rich layered oxides of similar crystal structure, $Li_{1.2}Ni_{0.2}TM_{0.6}O_2$ (TM = Mn, Ru), enable a similar amount of Li removal and uptake during the charge-discharge process, but with remarkably different charge profiles (voltage plateau at 4.55 volt (V) for TM = Mn versus a sloping profile for TM =Ru).

We capture the oxygen behavior ranging from O^{2-} in the crystal lattice to O^0 in the extreme case of O_2 gassing. From *operando* differential electrochemical mass spectrometry, these two compounds demonstrated very different gas evolution behavior, characterized by a total O_2 and CO_2 evolution of 0.2 and 0.3 µmol/mg, respectively, for TM = Mn versus negligible CO_2 or O_2 gas release for TM = Ru.

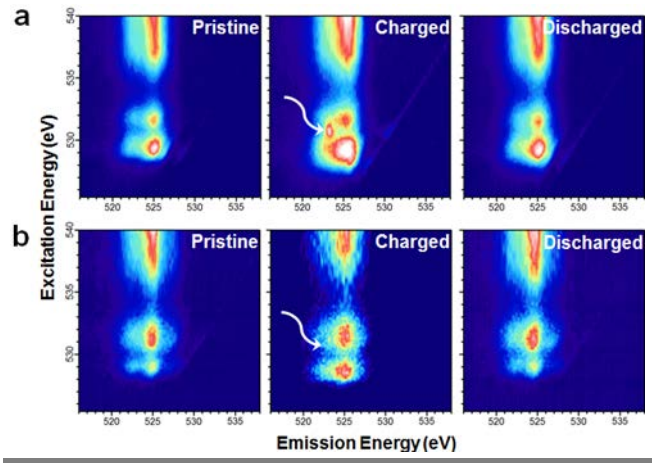

Figure 2. O K-edge RIXS maps of $Li_{1.2}Ni_{0.2}TM_{0.6}O_2$, (a) TM = Mn, (b) TM = Ru at various states of charge. The white arrow points to the specific O redox state that is absent in TM = Ru.

We further probe the intrinsic lattice O activity using resonant inelastic X-ray spectroscopy (RIXS). A striking RIXS feature appears (marked by white arrow) at the charged state of TM = Mn, and it disappears after 2.0 V discharge. However, no striking feature was observed for TM = Ru (Figure 2B). This unique feature, observed for the first time in our work, is direct evidence of the O state change (O redox) in the electrochemistry of $Li_{1.2}Ni_{0.2}Mn_{0.6}O_2$. This work provides a pathway to understanding and ultimately harnessing O redox to achieve high-capacity cathode materials and to understand the impact on cycle life.

2017 U.S. DRIVE Highlight

Commercially Scaled Approach to Produce Microporous Silicon for Lower Cost Lithium-Ion Batteries

The microporous structure addresses cycle life limitations of high-capacity silicon-composite anodes. Navitas used low-cost precursors, eliminated hazardous materials, and used industrially scalable processes.

Navitas Systems

Navitas Systems, with collaborators Argonne National Laboratory (ANL) and NexTech Materials, demonstrated a novel, commercially scalable approach to produce microporous silicon (µpSi). This program resulted in a significant reduction in the cost and environmental impact of high-capacity anodes that are needed to meet the U.S. Department of Energy's (DOE) battery cost goals. DOE's program advanced µpSi processes from a bench scale to a pilot scale production level.

Si nanocomposite materials have been identified as a promising anode technology for electric vehicle (EV) batteries. Presently, high-capacity Si-based anodes rely either on materials that are expensive (e.g., nano-Si powder) or on processes that are limited by low yield methods (e.g., chemical vapor deposition). µpSi potentially avoids these limitations and is attracting increasing attention as a lower-cost alternative for manufacturing high-capacity Si-based anodes. µpSi suitable for EV batteries is not currently available as a commodity material.

DOE has established a goal of $100/kWh system level cost for an EV battery. This cost target can be met with moderate risk through pairing Si-based high capacity anodes with lithium-rich nickel-manganese-cobalt-oxide cathodes. For this set of assumptions, the Si anode active material cost must be less than $25/kg. The Navitas µpSi powder manufacturing process reaches this target through a combination of low-cost commodity raw materials and reactants with scalable and low environmental impact processes. Processing involves mechanical milling and thermal reduction operations that are in wide application at industrial scale.

The impact of this program is a manufacturing process able to produce battery grade µpSi powder in high volume. The resulting material cost leaves ample overhead for post-processing and is still able to meet the 1,300 mAh/g (with low irreversible capacity loss, Figure 1) and $25/kg capacity and cost targets used in the BatPaC EV battery software. Recently, Navitas has demonstrated greater than 500 cycles (80% depth of discharge) in pouch full cells using a µpSi anode of 600 mAh/g and 3 mAh/cm^2 loading. By significantly increasing battery energy density and reducing battery cost, the proposed technology will stimulate EV adoption rate.

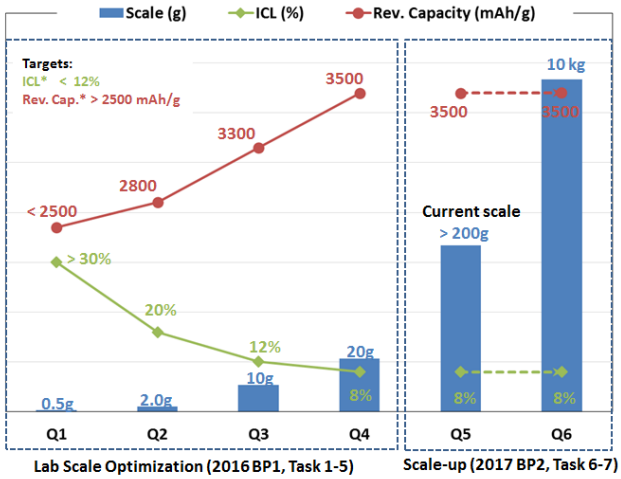

Figure 1. The key technical challenge met by Navitas was fully converting the oxide, as indicated by reaching near-theoretical capacity of pure Si, with minimal irreversible capacity loss (ICL) due to residual electrochemically active oxides. Processes were scaled from bench to multi-kg quantity using industrial processing equipment. Using oxide-based precursors with low-cost and non-hazardous reactants reduced product cost.

2017 U.S. DRIVE Highlight

High-Voltage Electrolytes for Lithium-Ion Batteries

High-voltage electrolytes reveal excellent resistance to high voltage degradation, improved cycle-life, and operation at elevated temperatures.

NOHMs Technologies, A123 Systems, Xerox, and the U.S. Advanced Battery Consortium

High-voltage lithium (Li)-ion batteries have the potential to enable low-cost and long-range electrified vehicles. A new class of high voltage cathodes, $LiNi_{0.5}Mn_{0.3}Co_{0.2}O_2$ (HVNMC), can deliver capacity greater than 250 mAh g–1, that is ~65% higher than that delivered by current state-of-the-art cathodes. Conventional Li-ion cells generally do not exceed 4.2 volt (V). To access higher capacities, the cell has to operate at a higher potential > 4.5 V versus Li/Li. Electrolyte stability at ≥4.5 V remains a major obstacle for enabling high voltage Li-ion chemistries.

The battery electrolyte plays a critical role, shuffling Li+ ions between the cathode and anode electrodes. When exposed to high voltages at the cathode surface, electrolyte components decompose. This results in capacity fade and a reduced cycle life. NOHMs Technologies has developed functional ionic liquid-based hybrid electrolytes that overcome these challenges, enabling high power, long cycle life, wide temperature range, and safer operation for high-voltage cells that will improve energy and power density of electric vehicle batteries. Specifically, NOHMs has developed electrolyte formulations that prove stable up to 5.0 V in high voltage $LiNi_{0.5}Mn_{1.5}O_4$ (NMO) cells and ≥4.5 V in HVNMC cells.

In addition to energy and cycle life improvements, NOHMs electrolytes demonstrated similar abuse tolerance compared to conventional electrolytes. NMO cells with the NOHMs electrolyte exhibited reasonable power capabilities, with cycling at 1C charge and 2C discharge (Figure 1). Cold temperature NMO performance demonstrated little to no shift in voltage during three cold crank tests at -30°C.

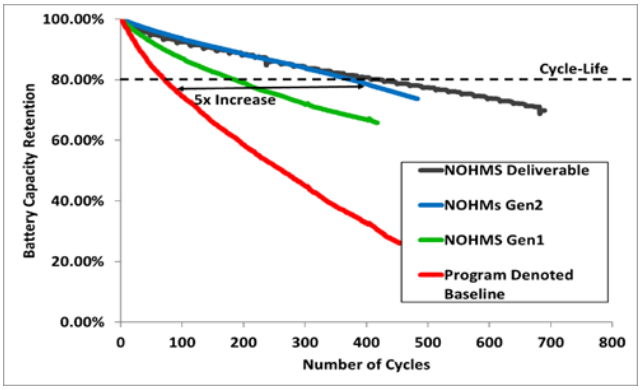

Figure 1. Cell discharge capacity performance of NOHMs Gen1, Gen2, and program denoted baseline in NMO|Graphite single layer pouch and NOHMs Deliverable electrolyte in 2 Ah NMO|Graphite pouch. Cells cycled at 23°C, using 1C charge, 2C discharge, and 3.4 V-4.8 V window.

Figure 2 shows the electrochemical performance of NMC cells with NOHMs electrolyte cycled at 23°C and 45°C. They both show good cycle performance of greater than 400 cycles at 4.5 V.

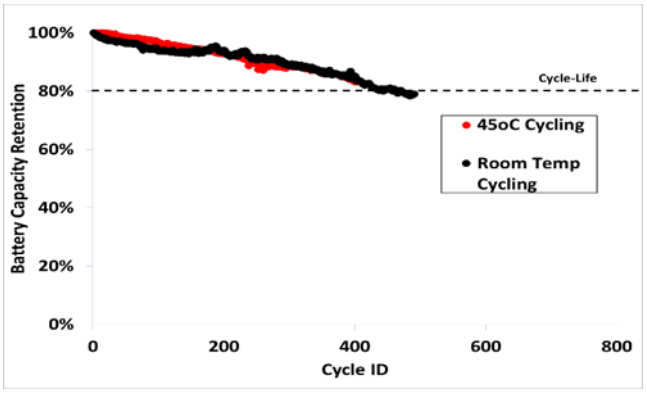

Figure 2. 45°C versus Room Temperature comparison of cells containing deliverable electrolyte. 155mAh NMC442 cells were cycled at C/2 with a 4.5 V cut-off.

NOHMs electrolytes have enabled high-voltage cathodes, improving energy density by 20% and reducing material cost.

2017 U.S. DRIVE Highlight

Low/Zero Volatile Organic Compound Processing of Thick, Crack-Free Electrodes

Oak Ridge National Laboratory has successfully solved cracking challenges in aqueous processing for thick electrodes. Low/zero volatile organic compound processing of thick electrodes offers the opportunity to produce lower-cost, higher-energy-density lithium-ion batteries.

Oak Ridge National Laboratory

Aqueous processing of thick electrodes with areal loadings much greater than 4 mAh/cm^2 (current state-of-the-art) for lithium-ion cells promises to increase energy density due to increased fraction of active materials, and to reduce cost due to eliminating the toxic N-methylpyrrolidone (NMP) solvent. An electrode with 12 mg/cm^2 loading made via aqueous processing is uniform and crack-free, but cracking becomes an issue for electrode coatings of 25 mg/cm^2 (Figure 1(a)). During electrode drying, capillary pressure builds up and local gaps widen due to increasing in-plane capillary forces. Eventually, the film cracks to release these stresses.

Scientists at Oak Ridge National Laboratory (ORNL) have developed a new processing approach by adding a small amount of low/zero volatile organic compound (VOC) co-solvent during aqueous electrode processing. This new method lowers the solvent mixture surface tension and associated capillary pressure during drying, thus eliminating cracks in thick electrodes. The critical thickness (or loading of the coating without cracking) increases when more co-solvent is used in the dispersion preparation, which is attributed to the further reduced solvent mixture surface tension. Figure 1(b) shows the coating quality improvement at 25 mg/cm^2 loading. It is crack-free and comparable to a conventional NMP solvent processed electrode (Figure 1(c)).

Pouch cells were assembled and tested at ORNL's Battery Manufacturing R&D Facility. Figure 1(d) shows cycling performance using different electrodes. The aqueous processed cracked electrode reaches 70% capacity retention after 620 cycles due to its poor coating quality. With isopropyl alcohol (IPA) addition to the formulation, improved cycling performance was obtained from electrode integrity improvement. The electrodes with water (H_2O)/IPA 9/1 and H_2O/IPA 8/2 solvent weight ratios retained 81.3% and 83.6%, respectively, which is comparable to the 83.0% retention for the NMP processed electrode after 700 cycles. We are currently researching the influence of hydrolysis of methyl acetate (MeOAc) on the cycling performance of the cathode processed with H_2O/MeOAc at a 9/1 solvent to weight ratio.

The influence of different processing aides on forming ground level ozone is estimated in Figure 1(e). For NMP processed electrodes, the kg/ozone per kg NMC 532 processed is 3.31, which is decreased by ~2 orders of magnitude with the ORNL low/zero VOC processing method. This benefit is particularly beneficial if no ozone reclamation or scrubbing is in place. This technology presents a rational strategy for thick electrode processing with low environmental impact while reducing processing cost and increasing energy density. Analyses estimate 5.5% cell cost savings (25% to 30% electrode processing savings) through using H_2O drying, and the cost of NMP solvent and its recovery.

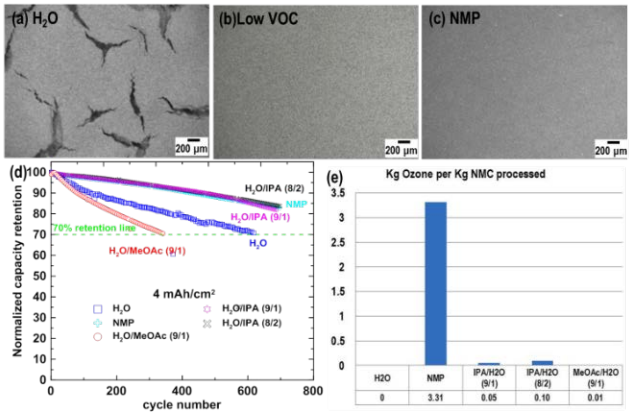

Figure 1. Scanning electron microscope images of NMC532 coating processing using (a) H_2O, (b) low VOC solvent and (c) NMP solvent. (d) Long term cycling performance of typical NMC532 electrodes from different processing methods in pouch cell at C/3. (e) Calculated ozone forming potential from different processing methods.

2017 U.S. DRIVE Highlight

Electrolyte Additive Enables Stable Cycling of Lithium-Metal Batteries

Specific low-concentration additives incorporated into a dual-salt electrolyte can stabilize a lithium-metal anode and enable the cells to be cycled for a longer time.

Pacific Northwest National Laboratory

Large-scale market penetration of electric vehicles (EVs) demands high-energy-density batteries beyond the current lithium (Li)-ion batteries. Rechargeable Li-metal batteries offer potential for such battery systems, but Li dendrite growth and low coulombic efficiency, especially at high charge current densities, have impeded the successful deployment of rechargeable Li-metal batteries for widespread adoption.

Researchers from Pacific Northwest National Laboratory have demonstrated that Li-metal anodes can be stabilized by adding a small amount of Li hexafluorophosphate ($LiPF_6$) into the dual-salt electrolytes of Li bis(trifluoromethanesulfonyl)imide (LiTFSI) and Li bis(oxalato)borate (LiBOB) in conventional organic carbonate solvent mixtures of ethylene carbonate (EC) and ethyl methyl carbonate (EMC). This electrolyte greatly enhances more rapid rate cycling and long-term cyclability of Li metal batteries. Li-metal cells using this electrolyte and a Li nickel-manganese-cobalt oxide (NMC) cathode retain a high capacity of 140 mAh/g at the 500th cycle at a high current density of 1.75 mA/cm^2 at 30°C, and 97.1% capacity retention (blue line in Figure 1a). As a comparison, Li||NMC cells with the conventional $LiPF_6$ electrolyte and the LiTFSI-LiBOB dual-salt electrolyte without $LiPF_6$ additive show fast capacity drop at about 60 cycles and 450 cycles, respectively. This $LiPF_6$-added dual-salt electrolyte enables the Li||NMC cells to maintain stable cycling for more than 400 cycles at 1.75 mA cm^{-2} at 60 °C as well as high rate charge and discharge capabilities (not shown). Interfacial resistance was found to increase only 25% in the $LiPF_6$ added dual-salt electrolyte, versus over 100% in the dual salt electrolyte, and 300% in the conventional electrolyte cases.

The cross-section views of the cycled Li-metal electrodes after 100 cycles show that the Li electrode in the conventional $LiPF_6$ electrolyte is seriously damaged (Figure 1b), while the Li electrodes in the two dual-salt electrolytes have little corrosion on the surface (Figure 1c, 1d). The addition of $LiPF_6$ additive in the dual-salt electrolyte further suppresses the surface degradation layer on the bulk Li metal electrode (Figure 1d). The post-analyses indicate that the $LiPF_6$ induces the generation of a robust and conductive solid electrolyte interface layer enriched with polycarbonate species on the Li-metal surface, mitigates the reduction of Li salts, especially LiBOB, and stabilizes the aluminum current collector of the NMC cathode.

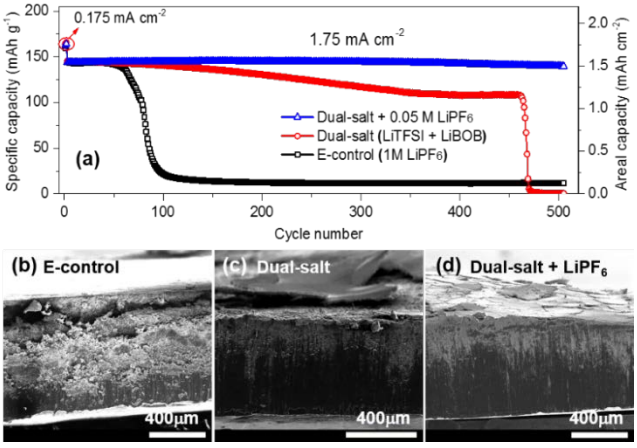

Figure 1. (a) Long-term cycling stability of Li||NMC cells with various electrolytes in EC-EMC solvent mixture at charge and discharge current density of 1.75 mA cm^{-2}. Cross-section views of cycled Li electrodes recovered from Li||NMC cells after 100 cycles using (b) conventional $LiPF_6$ electrolyte, (c) LiTFSI-LiBOB dual-salt electrolyte, and (d) 0.05 M $LiPF_6$ added dual-salt electrolyte.

2017 U.S. DRIVE Highlight

Enhanced Cycle Life Silicon-Based Anodes Support Long-Range Electric Vehicles

Porous silicon mixed with graphite extends cycle life and reduces swelling of silicon-based cells, which increases the energy density of lithium-ion batteries and extends the range of electric vehicles.

Pacific Northwest National Laboratory

Society's increasing demand for electric vehicles (EVs) has spurred extensive development of high-energy density lithium-ion batteries (LIBs). The silicon (Si)-based anode is a key technology that can deliver LIBs with specific energy of greater than 300 Wh/kg, increasing the range and decreasing the cost of EV batteries. However, significant swelling of Si-based anodes continues to be a critical barrier.

Researchers from Pacific Northwest National Laboratory developed a Si sponge with nano-sized pores and optimized the composition for enhanced cycle life. This work enables Si-based electrodes with extended cycle life and minimized swelling, which was demonstrated by in-situ electrochemical dilatometer testing in collaboration with General Motors. Figure 1a shows the charge/discharge (black curve) and electrode swelling (red curve) of a typical electrode with porous Si/carbon (C) and graphite ratio of 1:2. The initial electrode swelling is ~20% after full lithiation and ~7% after delithiation.

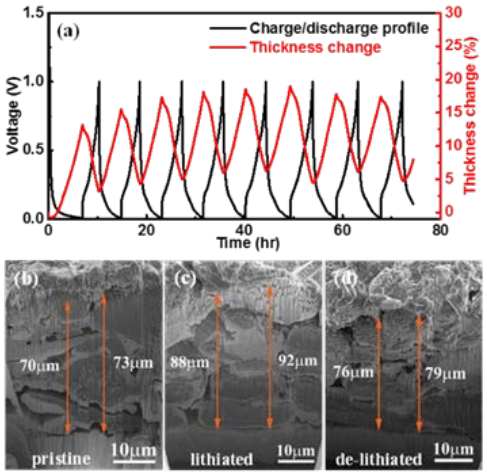

Figure 1. Characterization of the electrode swelling. (a) In-situ measurement of the electrode swelling upon discharge-discharge process. (b) SEM image of an electrode before cycling. (c) SEM image of a fully lithiated electrode after 10 charge/discharge cycles. (d) SEM image of a fully de-lithiated electrode after 10 charge/discharge cycles.

Figures 1b-1d are cross-section scanning electron microscopy (SEM) images of the electrodes before and after cycling. The electrode swelling at lithiated and de-lithiated state is 25% and ~11%. The electrode delivers a capacity of ~650 mAh/g (twice that of state-of-the-art graphite) and ~82% capacity retention over 450 cycles.

The Si/C-graphite||$Li(Ni_{1/3}Mn_{1/3}Co_{1/3})O_2$ full cell with a prelithiated anode provides greater than 84% capacity retention over 300 cycles at a practical loading level of ~3 mAh/cm^2, Figure 2. The team is now further developing low-cost and scalable approaches to synthesize the porous Si materials, exploring methodologies for practical prelithiation for high-energy LIBs for long-range EVs, and increasing the loading to enable higher energy cells.

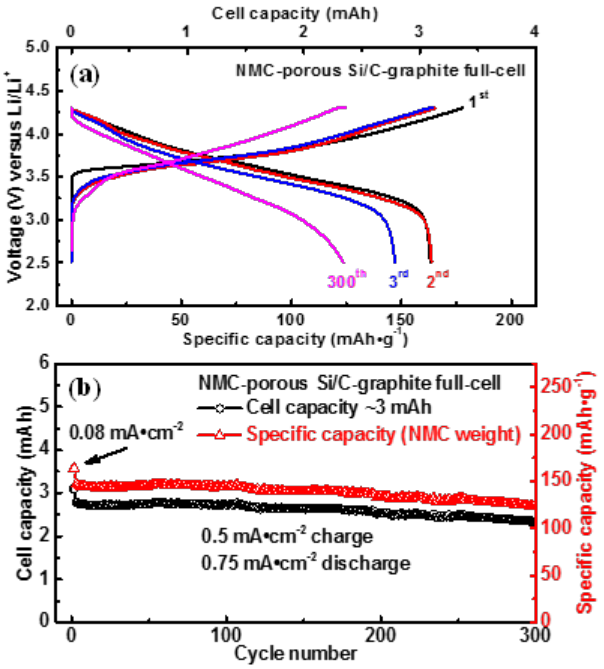

Figure 2. (a) Typical charge-discharge curves of the Si/C-anode versus the $Li(Ni_{1/3}Mn_{1/3}Co_{1/3})O_2$ cathode. (b) Long-term cycling stability of the electrode versus the $Li(Ni_{1/3}Mn_{1/3}Co_{1/3})O_2$ cathode. NMC is nickel-manganese-cobalt.

2017 U.S. DRIVE Highlight

Novel Surface Coating Enables High Active Material Electrode Loading and Excellent Performance

PSI developed an active material coating that results in a higher percentage of active material electrodes and more stable high voltage cycling.

Physical Sciences Inc.

Physical Sciences Inc. (PSI) has developed a technology that allows for higher energy density batteries by eliminating or reducing the amount of inactive, non-energy containing components used in traditional lithium (Li)-ion batteries, while maximizing the voltage range. Specifically, PSI has developed an active material coating technique that enables high active (HA) loading, at greater than 98 mass percent, cathode electrodes. Commercial Li-ion batteries, like those used in cell phones, typically have active material contents of 90-95 mass percent. In addition to increasing the energy by decreasing the amount of non-energy containing materials, this technology also allows for a much denser coating, thus increasing not only the energy per unit weight but also the energy per unit volume. Experimental testing in Li-ion pouch cells built with the HA technology has demonstrated the ability to increase the electrode mass loadings without reducing the power performance.

PSI's HA coating is a powerful tool that has been shown to be effective in not only increasing the loading and density of electrodes, but also in enabling stable high-voltage cycling. As shown in Figure 1, 3 Ah cells constructed with HA electrodes cycled at 4.4 volt (V) deliver very good cycle life (greater than 89% of the initial capacity after 1,000 cycles). These cells incorporate standard electrolyte components and utilized no prelithiation step. Modeling indicates that both cell level gravimetric energy density and volumetric energy density can be increased by as much as 17% and 22%, respectively, on utilization of HA electrodes at high voltages.

Incorporating PSI's HA technology increases cell level energy density, and reduces cost and waste during manufacturing, resulting in lower cost cells that can simultaneously meet the demanding cycle life and dynamic power requirements of next-generation electric vehicles.

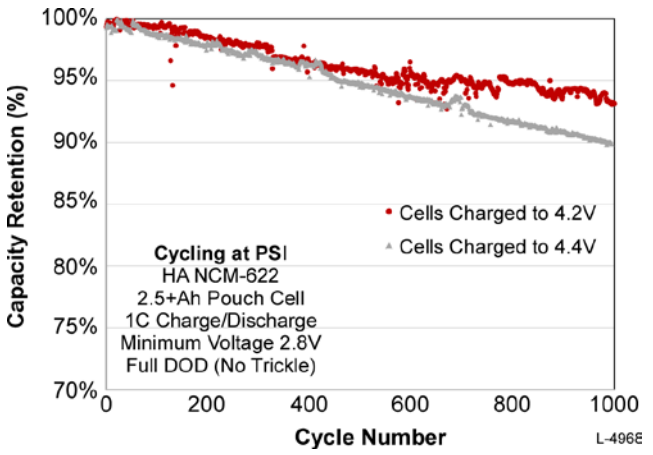

Figure 1. PSI HA cells cycled to 100% depth of discharge (DOD) and at 4.2 V and 4.4 V deliver more than 89% of the initial capacity after 1,000 cycles.

2017 U.S. DRIVE Highlight

Surface Protection on Three-Dimensional Lithium-Metal Anodes

Minimal volume change and effective surface protection are the keys for stable lithium-metal anodes. Stanford University has developed a facile surface coating using Freon reagent to form dense and conformal lithium fluoride protective surface on 3D lithium, which is crucial for lithium anodes cycling stability.

Stanford University

Lithium (Li) battery technology is the key for future automotive applications, which requires batteries with much higher energy density while maintaining long cycle life. One promising approach to high energy is to use Li-metal as the anode. Consequently, developing stable Li-metal anodes has been an important prerequisite to viable high-energy battery systems for electric vehicles.

However, several challenges, including poor cyclability and Li dendrite formation, need to be overcome before Li-metal anodes can become viable. Behind these problems, there are more essential issues in play, namely, the infinite relative volume change of the electrodes during cycling and high reactivity of metallic Li. In this consideration, spontaneously realizing minimal volume change and conformal surface protection is required.

Scientists at Stanford University, who earlier innovated composite Li anodes with minimal volume change, have recently developed a facile surface Li-fluoride (LiF) coating technique that can conformally passivate three-dimensional (3D) surfaces of the composite Li anodes. The technique involves Freon R134a (1,1,1,2-Tetrafluoroethane) as the gaseous reagent, which exhibited multiple distinguished merits: 1) the gaseous Freon exhibits high permeability to coat the 3D surface conformally; 2) Freon 134a is low cost and commercially available; and 3) in contrast to the highly hazardous HF and F_2 gaseous reagents, Freon 134a is non-toxic and friendlier to the environment.

By exposing metallic Li to Freon R134a (Figure 1a,) assisted with controlled pressure and temperature, a LiF layer with tunable thickness was first coated directly onto metallic Li, with a thickness of ~ 40 nm (Figure 1b). The thin LiF coating is dense and conformal so that the protected Li can survive ambient air exposure while the unprotected Li is easily corroded. A conformal LiF film was then coated onto layered Li-reduced graphene oxide (Li-rGO) composite anode (Figure 1c), which can offer further improved interfacial stability in addition to its highly reduced relative volume change. Although the gas reaction byproducts were not detected here, the expected products are not harmful.

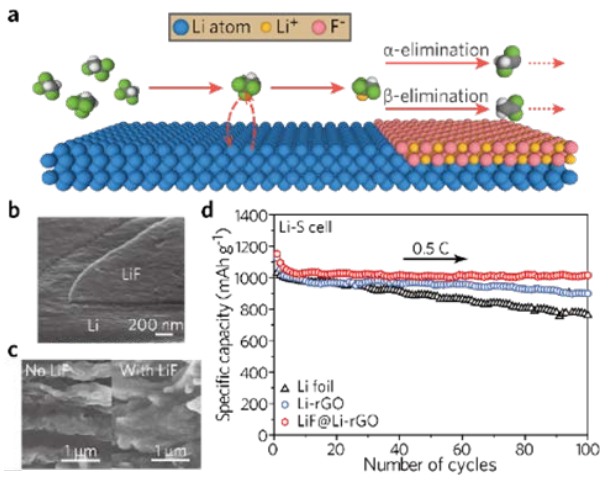

Figure 1. (a) Proposed chemical reaction between Li and Freon gas molecules. (b) Cross-section scanning electron microscope image showing the conformal LiF coating on Li surface. (c) Comparison of Li-rGO composite electrode before (left) and after (right) LiF coating. (d) Comparison of cycling stability in Li-S cells using bare Li foil, Li-reduced graphene anode, and LiF coated Li-reduced graphene oxide anode.

Symmetric-cell cycling corroborated the enhanced stability with LiF coating, with negligible voltage fluctuation or resistance increase over 200 cycles. Further, Li-sulfur cells with LiF-coated layered Li-rGO as the anode exhibited improved cycling stability (Figure 1d) and coulombic efficiency (~99%), confirming good surface passivation and thus reduced shuttle effect. This work demonstrates a promising approach to stabilize Li-metal anode by further passivating a 3D Li composite anode, which may increase the potential for a viable and higher cycle life Li-metal-based rechargeable battery.

2017 U.S. DRIVE Highlight

Surface Treatment Enables Higher Rate Capability and Critical Current Density in Lithium-Metal Anode Cells

Solid-state batteries could double the energy density of conventional lithium-ion batteries. Among other issues, demonstrating charging rates comparable to lithium-ion batteries has been a challenge. In this study, a process was developed to enable high charge rates in solid-state batteries.

University of Michigan

Transitioning from a fossil fuel-based economy to one based on renewable resources creates the impetus to develop energy storage technology with higher energy density, enhanced safety, and reduced cost. Lithium-ion batteries (LIBs) are promising for near-term energy storage needs; however, for vehicle electrification, a step-change increase in battery performance could further accelerate large-scale adoption.

Toward this goal, a tangible increase in energy density may be achieved through the development of solid-state batteries (SSB). Instead of relying on liquid electrolytes to transport ions, SSBs use a solid electrolyte. Over the last two decades, several solid electrolytes were discovered. One class of ceramic solid in particular, based on the garnet atomic structure, exhibits a good combination of rapid ion transport and stability. These attributes may enable the use of the holy grail of electrodes, metallic lithium (Li). However, interfacial impedance between the Li-metal and solid electrolyte has been a major impediment.

Typically, metals do not bond to ceramics, including the garnet class of solid electrolytes, LLZO. Researchers have recently studied coatings to enhance interfacial properties between Li and the LLZO. However, coatings could complicate manufacturing and may degrade with cycling.

Ideally, bonding between Li and the solid-state electrolyte should be achieved with no coating. This was recently demonstrated through a simple heat treatment (1 hour at 400 ˚C-500˚C) that cleans the LLZO surface to allow bonding between metallic Li and garnet (Figure 1, top). Moreover, achieving sufficient bonding results in a lower impedance interface, which in turn enables a more rapid rate capability in solid-state batteries (Figure 1, bottom).

This achievement demonstrates the importance of fundamental experimental and theoretical studies working in concert to understand complex phenomena. By exploiting this fundamental knowledge, researchers have shown that the speed at which Li ions pass through a solid-state interface is comparable to state-of-the-art LIBs using liquid electrolytes. These findings could accelerate the development of advanced SSBs that provide a significant increase in the energy density of conventional LIBs.

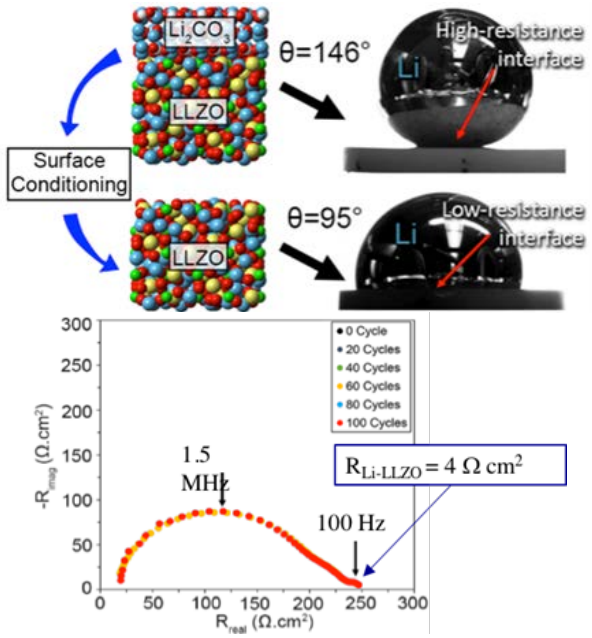

Figure 1. Top. Evidence that Li-metal can bond to a ceramic solid electrolyte is confirmed by theory (left) and experiment using a wetting test (right). Without cleaning, the LLZO surface is passivated by Li carbonate, and molten Li (at 200°C) does not wet the LLZO surface. By removing the Li carbonate via heat treatment, molten Li wets the LLZO. Bottom. Heat-treated LLZO has reduced interfacial impedance to 4Ω and cell impedance (mainly from bulk LLZO) to 254Ω, and remains stable over 100 cycles. The interfacial resistance without heat treatment is 300-400 Ω-cm^2.

2017 U.S. DRIVE Highlight

Improved Energy and Cycling Stability of Lithium-Sulfur Cells through Polysulfide Trapping

Newly developed binder-free sulfur cathodes enable very high sulfur loadings, and high discharge capacities, four to five times greater than commercial insertion based cathodes. In addition, polysulfide trapping agents result in greatly enhanced cycle life.

University of Pittsburgh

Lithium (Li)-sulfur cells offer double the energy density of current Li-ion cells. However, thick sulfur cathodes are difficult to utilize due to their poor electrical conductivity, and cycle life continues to suffer partially due to polysulfide dissolution and reaction with the Li-metal anode. We have developed a directly doped sulfur architecture (DDSA) electrode with high sulfur loadings of ~18 mg/cm^2, (~20 mAh/cm^2), three times higher than that of slurry-coated oxide electrodes. Researchers prepared the DDSA electrodes using a scalable electrodeposition approach for depositing sulfur from an aqueous solution onto a carbon fiber substrate (which is also used as a current collector). The DDSA electrodes are then coated with polysulfide trapping agent (PTA) that binds polysulfides and prevents their entry into the electrolyte. Density functional theory (DFT) calculations performed on a spectrum of materials that can potentially bind polysulfide species served as the basis for the selection of the PTAs used here.

Both the DDSA electrodes and PTA-coated DDSA electrodes were tested in coin cells against a Li-metal anode and using a standard liquid electrolyte. The team compared cycling performance of the slurry-coated commercial sulfur cathodes with that of the DDSA and PTA coated DDSA electrodes (Figure 1). The commercial sulfur cathode displays an initial capacity of 557 mAh/g, which rapidly fades to 100 mAh/g in ~60 cycles. However, the DDSA electrodes, despite high electrode loadings, showed a high initial capacity of 1,088 mAh/g and maintained 809 mAh/g for 200 cycles. The PTA-coated DDSA electrode also displays excellent electrochemical cycling response, showing an initial capacity of 1,305 mAh/g stabilized at 1,112 mAh/g after 200 cycles at 0.2C rate. The initial ~0.2% fade is likely due to parasitic reactions; the team will attempt to overcome this by further optimization.

Ultraviolet-visible spectroscopy analysis of the electrolytes before and after 200 cycles showed considerable decrease in the intensities of peaks corresponding to higher and lower order polysulfides as opposed to the slurry coated sulfur cathodes, indicating the effectiveness of the technology for improved cycling stability.

The team also performed X-ray photoelectron spectroscopy (XPS) analysis on the PTA-coated DDSA electrodes and slurry-coated sulfur electrodes after 200 cycles to understand the origin of the cycling stability of these cathodes. The XPS spectrum of PTA-DDSA lacks peaks corresponding to higher and lower order polysulfides observed in slurry coated electrode. This confirms the effectiveness of PTA-DDSA electrodes in mitigating and trapping polysulfides. The PTA-coated DDSA electrodes thus largely eliminates the polysulfide dissolution problem in Li-sulfur batteries.

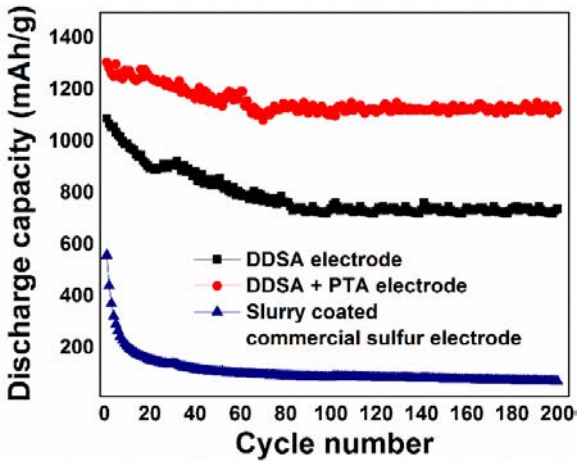

Figure 1. Electrochemical cycling performance of the DDSA electrode and PTA-coated DDSA electrodes (~18 mg/cm^2 sulfur loading) compared with slurry coated commercial sulfur electrode.

Fuel Cells

2017 U.S. DRIVE Highlight

Potential Cost Savings Identified in System Model

Fuel Cell System model highlights cost-saving options, and enables operating condition regimes, that have the potential to significantly reduce automotive fuel cell system cost via removal of expensive components.

Argonne National Laboratory

The U.S. Department of Energy's (DOE) fuel cell research focuses on enabling materials and advancing understanding of fundamentals to achieve higher performance (and more cost-competitive) fuel cell technologies. A validated fuel cell model is an essential tool for gauging the progress in research and development activities and identifying opportunities for further improvement in performance and cost. Argonne National Laboratory (ANL) continues to develop and validate an integrated model for automotive systems using data from DOE-funded projects and input from a wide range of stakeholders. The model can help assess component performance in an integrated system, optimizing operating conditions for performance and cost; supports DOE in setting technical targets and directing component development; and provides data and specifications for the annual manufacturing cost update.

In the past year, ANL identified three approaches with potential to significantly reduce cost and improve system power density (packaging):

1. Developed and validated models projecting de-alloyed platinum/nickel dispersed cathode catalyst electrodes that could achieve DOE's 0.125 g/kW target and exceed DOE's 1,000 W/cm^2 power density target, while still meeting automotive system operating constraints (e.g., hill climb requirement). With the model-optimized operating conditions, ANL projected a substantial reduction in system cost, from $53/kW to $45/kW.

2. Investigated the potential to remove the air humidifier component and identified operating conditions resulting in virtually no loss in stack power density, while still allowing for the high-temperature operation necessary to meet automotive hill climb requirements (~95°c operation). This change not only reduces cost, but reduces system packaging volume.

3. Using computational fluid dynamics, the team demonstrated that the hydrogen recirculation blower may be eliminated by using a pulsed ejector and identified operating control requirements (maximum allowable nitrogen concentration) to avoid electrode degradation from fuel-starvation. Potential benefits include $3 to $5/kW cost savings, volume reduction, and improved reliability via reduction in moving parts.

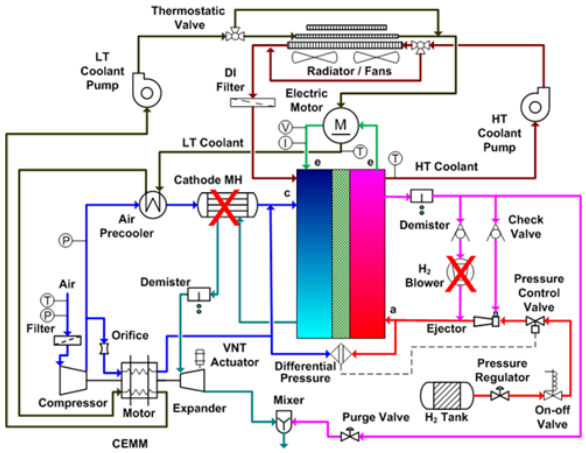

Figure 1. 2016 ANL FCS system highlighting potential eliminations with proper system design and operating conditions.

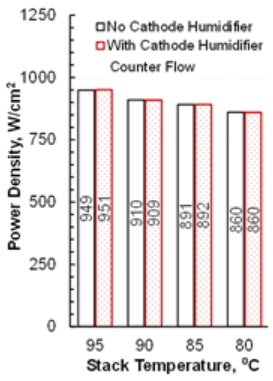

Figure 2. Highlights operating conditions (pressure, anode stoichiometry, counter-flow anode/cathode) that enable removal of humidifier component without performance penalty at target T (~95°C). ≥2.5 atm pressure, anode stoichiometry=2, anode counter-flow to cathode, 14μm or thinner membrane.

2017 U.S. DRIVE Highlight

2020 Target for Power Output per Gram of Precious Metal Surpassed

Improved accessibility to the platinum catalyst provides higher power for the same amount of platinum and same size fuel cell, lowering cost.

General Motors

Precious metals, also known as platinum group metals (PGM), including platinum (Pt), are one of the major contributors to fuel cell cost. Reducing Pt content by increasing catalyst activity has been a major research focus area. This effort has been successful, and has increased the activity of Pt alloys, surpassing the U.S. Department of Energy's oxygen reduction reaction (ORR) activity target. However, the performance at high power, which determines the overall size and cost of a fuel cell, has not improved as rapidly and falls short of targets. GM, in partnership with Cornell University (CU), Carnegie Mellon University, Drexel University, National Renewable Energy Laboratory, and 3M Company, has addressed this shortcoming by focusing on the catalyst support, and have improved performance at high power with low Pt loading alloy catalysts. The team has increased specific power from 8 kW/gPt at the start of the project to 14.3 kW/gPt. This increase in Pt utilization is largely responsible for reducing the estimated cost for an automotive fuel cell from $53/kW in 2016 to $45/kW in 2017.

As Pt content and catalyst surface area in the cathode are reduced, the same amount of reactants (oxygen and protons) must now be delivered to a smaller Pt surface area. For Pt loadings approaching less than 0.1 mg Pt/cm^2, this causes a performance loss due to relatively high local transport resistances near the catalyst particle in state-of-the-art electrodes. GM has developed carbon supports to allow a decrease in local transport resistances and increase power output under high-power operating conditions.

The carbon support has a strong influence on catalyst properties. A porous, high-surface area carbon (HSC) support enables good dispersion of the catalyst, high catalyst activity, and the preparation of good alloy catalysts. However, some of the Pt particles will be located within HSC pores and reactants may have limited access to them (see Figure 1A). A solid carbon provides better stability and positions the Pt at or closer to the surface, which minimizes local oxygen and proton resistances, but has lower surface area. A good balance between activity, accessibility, and durability is needed.

GM developed several different carbon supports and characterized the carbons and resulting supported catalysts and membrane electrode assemblies (MEAs). In collaboration with CU, the team developed a CO stripping technique that quickly determines the location of Pt (inside the pores or on the surface of carbon particles). MEA performance correlated with the pore size distribution of the carbon or catalyst powder. High ORR activity and low local transport resistances were associated with carbon supports that had more mesopores with appropriate size (4-7 nm) and fewer micropores (less than 4 nm). ORR activity dropped drastically for particles with no micropores, indicating ionomer poisoning when all the Pt is on the surface. GM demonstrated that balance must be achieved between easy access to the reactants and interactions with the ionomer. Future work will focus on ionomer-catalyst interactions and durability.

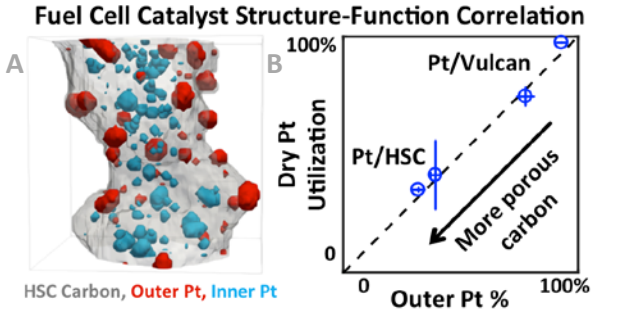

Figure 1. (A) Cryo-scanning transmission electron microscopy 3D tomograms showing location of Pt nanoparticles inside and outside of HSC particles. (B) Fractions of outer Pt particles as determined by TEM tomography (Outer Pt %) and by electrochemical CO stripping measurements (dry Pt Utilization).

2017 U.S. DRIVE Highlight

Sources of Mass Transport Resistance Related to Materials and Operating Conditions

Fuel cell testing used to show that oxygen mass transport resistances at low precious metal loadings relate directly to available surface area and how tortuous the path is for an oxygen molecule.

Fuel Cell Performance and Durability Consortium

To lower the cost of fuel cell stacks, one objective of fuel cell researchers has been to lower the precious metal catalyst content in a stack. Another objective has been to increase the stack's power density, which would decrease stack size and cost. However, at lower precious metal loadings, increased mass transport losses have been observed, which prevent operation at higher power density.

The Fuel Cell Performance and Durability (FC-PAD) Consortium involves multiple national laboratories leveraging their unique capabilities. The National Renewable Energy Laboratory (NREL) has been leading work within FC-PAD to define how materials and operating conditions affect the mass transport losses at the local interface with precious metal particles. Lawrence Berkeley National Laboratory, another FC-PAD laboratory, has been instrumental in carrying out this work with assistance from Oak Ridge National Laboratory (ORNL) on microscopy.

Prior work showed that mass transport losses related to oxygen diffusion through pores of 100 nm or greater throughout the electrode could be distinguished from other mass transport losses. The former losses are referred to as pressure-dependent losses, while the latter are referred to as pressure-independent losses. While efforts to lower the precious metal loading did not generally affect the pressure-dependent losses, lower loadings increased pressure-independent losses. The pressure-independent losses need to be addressed to realize high power density at low loading.

NREL's efforts expand on prior work that derives a local oxygen transport loss (R_{O2}^{Pt}) from a plot of pressure-independent losses versus electrode roughness factors. While some work is still needed to define the mechanism behind the local transport loss, it is generally understood that ionomer and nanoscale carbon particle pore hierarchies offer substantial resistance to the movement of an oxygen molecule to the surface of platinum (Pt) catalyst. NREL measured local resistances for Pt supported on the outside of a relatively non-porous carbon (Vulcan), as well as for Pt supported on a porous carbon (HSC), as shown in Figure 1. The results showed that a less tortuous path for oxygen lowered the resistance. Results also showed that higher relative humidity (RH) also lowered local resistances. Differences in resistances between the two carbons are less pronounced at low RH after normalizing for the actual electrochemical surface area.

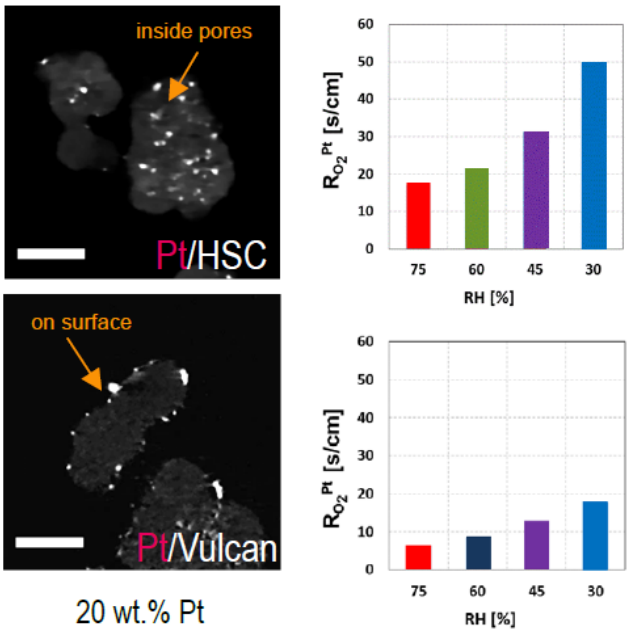

Figure 1. Local oxygen transport losses are shown to be lower for Pt supported on Vulcan carbon (bottom) versus Pt supported on HSC. (top) The Vulcan carbon situated Pt nanoparticles on the exterior of carbon particles, allowing easier transport of oxygen. Microscopy provided by ORNL.

2017 U.S. DRIVE Highlight

Performance Loss Mechanism of Fuel Cell Catalysts Identified

Advanced microscopy and mass spectrometry reveals correlation between the performance loss of platinum cobalt alloy catalysts and catalyst durability in operating fuel cells.

Fuel Cell Performance and Durability Consortium

Electrocatalyst stability is one of the primary factors dictating fuel cell lifetimes. The Fuel Cell Performance and Durability (FC-PAD) Consortium analyzes state-of-the-art (SOA) alloy catalyst materials to understand their stability under relevant fuel cell operating conditions. FC-PAD members Oak Ridge National Laboratory and Argonne National Laboratory used advanced microscopy, X-ray scattering and spectroscopy methods, and inductively coupled plasma mass spectrometry (ICP-MS) coupled with a flow-through liquid electrolyte electrochemical cell to study the stability of platinum (Pt)-based alloy electrocatalysts before, during, and after electrochemical testing. Recent evaluation efforts are focused on SOA platinum cobalt (PtCo) alloy catalysts acquired from several sources (varying Pt:Co compositions ranging from 15% to 30% Co). While PtCo is one of the highest performing alloy catalysts in terms of specific activity, it also exhibits significant performance loss during normal fuel cell operation. Thus, the primary goal of FC-PAD research is to understand the mechanism(s) contributing to PtCo degradation.

Researchers studied electrocatalyst degradation due to dissolution of Pt and Co, and the effect of voltage on this degradation pathway, using ICP-MS. Membrane electrode assemblies (MEAs) were prepared with PtCo/C catalysts incorporated in the cathode catalyst layers (CCLs). The team exposed MEAs to a catalyst cycling accelerated stress test (AST), e.g., 0.6-1.0 volt (V) triangle-wave potential cycling for 30,000 cycles. The following lists observations from ICP-MS and microstructural characterization of the PtCo/carbon (C) catalysts, before and after cycling:

1. ICP-MS results showed that Co was unstable and dissolved at all voltages. Pt dissolved at more than 0.8 V during both increasing and decreasing voltage profiles (Figure 1).

2. Analytical scanning transmission electron microscopy (STEM) was used to track Co migration from the CCL into the membrane.

3. Co dissolved ionically in the membrane and was homogenously distributed across the membrane thickness. Pt migration from the CCL, on the other hand, was characterized by the formation of a localized “Pt-band” in the membrane close to the CCL (Figure 2).

Quantifying Co leaching into the ionomer (in both CCL and membrane) is part of future work designed to quantify catalyst stability in the fuel cell. Recently, FC-PAD member Los Alamos National Laboratory also developed a new square wave potential cycling protocol that shortens the AST duration, allowing faster evaluation of advanced catalysts’ durability.

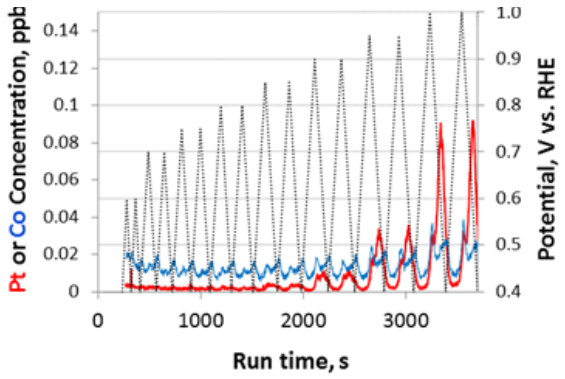

Figure 1. Voltage cycling with increasing upper limit shows Pt (red) and Co (blue) dissolution profiles (Pt_3Co /C).

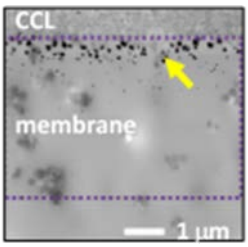

Figure 2. Cross-sectional STEM image of MEA with Pt_3Co/C CCL. An accumulation of large Pt particles form a Pt-band (yellow arrows) in membrane adjacent to CCL (purple dashed lines). Co is homogeneously distributed across full membrane thickness.

Materials

2017 U.S. DRIVE Highlight

Close Proximity Electromagnetic Carbonization

Development of a lower-cost, less-energy-intensive method for converting precursors into carbon fiber.

Oak Ridge National Laboratory

Carbon fiber (CF) is used in composite parts mostly for structural applications because of its low density, high strength, and modulus. However, use of this material was limited to the aerospace and defense industries until the late 1990s, when its cost began to decrease. The U.S. Department of Energy and Oak Ridge National Laboratory (ORNL) are currently pursuing a strategy for further cost reduction of CF manufacturing during the carbonization stage. Lower-cost precursors and composite production methods are under development, and a less expensive oxidative stabilization process is being commercialized.

The carbonization stage of the conversion process (highlighted in green in Figure 1) consumes a significant amount of energy. The current state-of-the-art still uses traditional high-temperature furnaces that heat the fiber, interior walls, and gases. A much more energy-efficient approach would directly couple the heat to the fiber and nothing else.

In 2013, RMX Technologies and ORNL experimental work led to an initial furnace prototype that demonstrated possible carbonization of oxidized polyacrylonitrile (PAN) fiber in the near field of antennas using radio frequency power. However, the carbonized area was not uniform.

In 2016, the team initiated the Close Proximity Electro Carbonization project to demonstrate over a 3-year period commercial viability of the furnace concept, and a cost reduction of the concept's carbonization stage such that large-scale industrial adoption would be achieved (production of 1,500 annual metric tons or more).

Project objectives are to:

- Reduce unit energy consumption (kWh/kg) by 50%,
- Reduce operational costs by 25%,
- Produce the same or better quality carbon fiber, and
- Scale the technology to a nameplate capacity of 1 annual metric ton and demonstrate by project end date.

In 2017, the effort focused on characterizing the material and on a computational electromagnetic (CEM) model. The team used the model to design the antenna equipment and the electromagnetic fields they radiate, and to predict temperature rise of the material. The team constructed a second physical setup at the end of the first year.

Operation of this setup led to successful continuous runs by the end of 2017. The project is using the data collected and the knowledge acquired for each parameter to design and model the next scaled furnace, which will have a nameplate capacity of 1 metric ton per year. The team studied two new types of electromagnetic applicators using the CEM model. For fabrication, scalability, and reliability purposes, the team selected a design that will be used in the next setup, the construction of which will begin in early 2018.

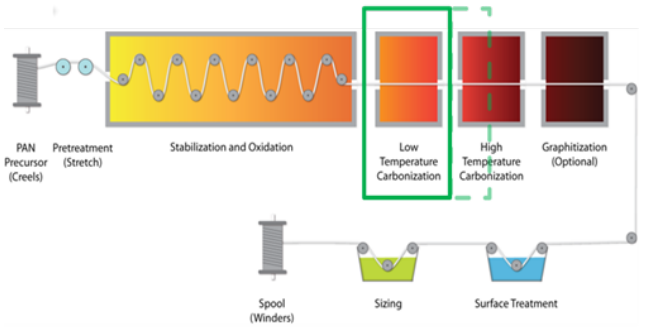

Figure 1. Flow diagram of the conventional PAN–based carbon fiber conversion process. The highlighted carbonization stage is the focus of this project. The low-temperature stage is the main focus (solid line), but the high-temperature stage is partially covered as well (dashed line).

2017 U.S. DRIVE Highlight

New Insights into Magnesium Corrosion

The discovery of rapid hydrogen transport into magnesium alloys exposed to water at room temperature provides the basis to better understand and potentially engineer magnesium alloys with improved resistance to hydrogen embrittlement and stress corrosion cracking.

Oak Ridge National Laboratory

Inadequate corrosion resistance is a key limiting factor to more widespread adoption of magnesium (Mg) alloys to achieve vehicle lightweighting targets for improved fuel economy. However, significant gaps exist in the understanding of the science behind Mg alloy corrosion. At Oak Ridge National Laboratory (ORNL), researchers are employing advanced electron microscopy, neutron scattering, and isotopic tracer characterization tools to gain fundamental knowledge needed for the successful design of more corrosion-resistant Mg alloys and coatings. The project is being pursued in collaboration with a Mg alloy producer, a coating producer, a Tier 1 automotive supplier, and three universities.

In 2017, the project team discovered that exposure of Mg alloys to water at room temperature resulted in an unexpectedly rapid diffusion of hydrogen (H_2) from the water into the alloy (up to 100 microns deep after only a few hours), as shown in Figure 1(a). This rapid H_2 penetration was found to be associated with small additions of zirconium (Zr) or neodymium (Nd) to the Mg, which are used in several commercial classes of Mg alloys to improve manufacturability and mechanical properties, as shown in Figure 1(b).

Preferential penetration and segregation of H_2 species was observed at interfacial regions of high Mg/Zr/Nd nanoprecipitate density and at Mg (Zr) metastable solid solution microstructural features. The ingressed H_2 was further found to be present in the alloy as nanoconfined, molecular H_2. These findings will have significant impact not only on better understanding of stress corrosion cracking (SCC) and related H_2 embrittlement attack of Mg alloys, but also on the development of new strategies to mitigate such detrimental phenomena. For example, the observed gettering of H_2 to Zr/Nd-rich nanostructure features could potentially be engineered to reduce the susceptibility of the adjoining Mg matrix phase to SCC. It is likely that other similar alloys, as well as the chemistry, size, and distribution of second phases that are formed, will significantly impact the H_2 ingress phenomena during aqueous corrosion. These findings were recently published in the journal *ACS Applied Materials and Interfaces*[1] and received the Light Metals Division Magnesium Technology Best Poster Award from the Minerals, Metals & Materials Society in 2018.

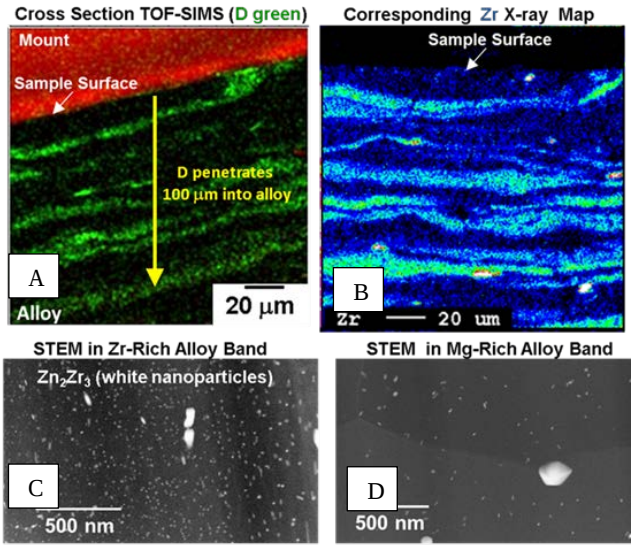

Figure 1. Evidence of SCC and H_2 embrittlement in Mg. Mg-1.5Zn-0.25Zr-<0.5Nd wt.% alloy ZE10A after 4 hours in deuterated water (D_2O). D segregates to Zr-rich alloy bands with high-density of Zn_2Zr_3 nanoparticles. TOF-SIMS: Time-of-Flight Secondary Ion Mass Spectrometry STEM: Scanning Transmission Electron Microscopy.

[1] M. P. Brady, et al., *Rapid Diffusion and Nanosegregation of Hydrogen in Magnesium Alloys from Exposure to Water*, ACS Applied Materials and Interfaces, 9 (43), 38125–38134 (2017).

2017 U.S. DRIVE Highlight

Solid-State Spot Joining of Aluminum Alloy to Advanced High-Strength Steel at Prototype Scale

Development of a solid-state spot joining technology to join 7xxx/6xxx series high-strength aluminum alloy and advanced high-strength steel for near-production readiness.

Oak Ridge National Laboratory

This project aims to develop, mature, and validate near-production readiness of a solid-state spot joining technology to join prototype-scale automotive body-in-white subsystems made of advanced high-strength steel (AHSS) and 7000/6000 series high-strength aluminum (Al) alloys (HSA alloys) for high-volume production. Researchers used two emerging solid-state, friction-heating-based spot joining processes—friction bit joining (FBJ) and friction stir spot welding (FSSW)—to join AHSS to Al alloys at a coupon scale. The project is led by Oak Ridge National Laboratory, with participation from an automotive original equipment manufacturer (OEM), materials suppliers (Tier 1 and Tier 2), and universities.

Development of the FBJ process focused on mass production using the final target material combination (7xxx HSA alloys and AHSS) and low-cost joining bit materials. Mechanical joint performance of the final target material combinations successfully met or exceeded all evaluation criteria set by the OEM and industry partners for cases without adhesive bonding (Table 1). However, adhesive bonding and weld-bonding (FBJ + adhesive) processes were also developed and met the assessment criteria.

Evaluation criteria	Target value (kN)	Test value (kN)
Tensile shear	>5	10.7
Cross-tension	>1.5	4.8
T-peel	>1.5	1.89
Fatigue (10^7 cycles)	0.75	Pass

Table 1. Summary of FBJ performance under coupon level testing.

The FSSW process was optimized to improve mechanical joint strength. Tensile shear strength was much higher than the strength values (2.0–4.0 kN) as reported in open literature for Al-to-steel FSSW of similar thicknesses. Weld-bonding (FSSW + adhesive) was also successful in that it exceeded the strength specified by the OEM.

FBJ process modeling was developed for a better understanding of thermal deformation histories during the joining process, depicting material flow approximating cross-sectional joint appearance. This model was used as a prerequisite to subsequent weld microstructure and performance modeling, and to understand the effect of temperature rise due to joining and thermal expansion mismatch of two different materials. The development of component-level modeling focused on understanding part distortion of the bimetallic structure during the paint-bake process, due to the mismatch of thermal expansion coefficients. Five joint configurations were modeled with their configurations modified to minimize paint bake distortion. The team then built and experimentally tested the fifth configuration. Figure 1 shows the configuration five model, the experimentally measured data, and the previous four model predictions.

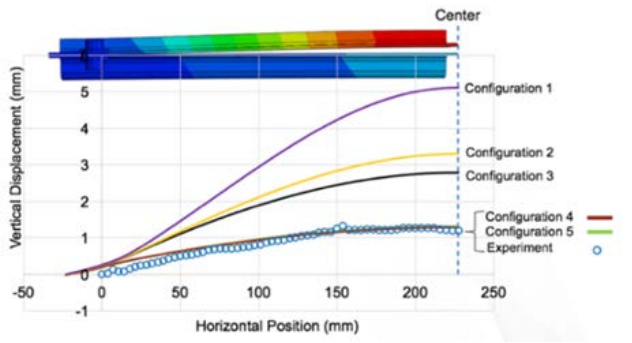

Figure 1. Distortion of the Al part taken from the centerline of the bimetallic structure for different joint configurations.

The project is now at the demonstration stage. Near-production-ready hardware for automotive high-volume production and prototypical body structure components have been produced and tested for mechanical strength and corrosion performance.

Enhancing Sheared Edge Stretchability of AHSS/UHSS through Integrated Manufacturing Process Simulations

The project targets developing a quantitative understanding of how microstructure affects the sheared edge fracture and stretchability of advanced high-strength steels/ultra-high strength steels, which helps accelerate implementation.

Pacific Northwest National Laboratory

During cold stamping of advanced high-strength steel (AHSS)/ultra-high strength steel (UHSS) parts, the most commonly observed failure mode is splitting at the edge of the sheet, where shearing has occurred. Sheared edge stretchability depends on various factors including material microstructure, blank preparation processes, die wear, and edge loading conditions. Quantitative and predictive capabilities linking the microstructure characteristics to the sheared edge stretchability are not available to modelers and designers. The purpose of this project is to enhance the sheared edge stretchability of AHSS/UHSS by developing quantitative and predictive understandings of the microstructure effects on sheared edge fracture and stretchability. This project has adopted a combined experimental and modeling approach. Researchers selected two DP980 steels from different suppliers (i.e., DP1 and DP2) as the model steel, and the overall approach should be extendable to other AHSS/UHSS grades.

The team performed hole-punch tests and tensile stretchability tests with these steels over a wide range of cutting clearances (i.e., distance between the punch and die). Researchers performed high-energy X-ray diffraction tests to evaluate the constituent phase properties. DP1 steels show better sheared edge stretchability compared to DP2 steels, and this is believed to be due to less phase strength disparity. Researchers observed a substantial difference in the effect of cutting clearance between the uniaxial tensile tests and the hole expansion tests (see Figure 1 for example). This is attributed to the difference in cutting conditions between punching a small hole and shearing along a straight line. Both tests provide essential information for designing stamping dies.

Researchers developed computational models and schemes for simulating both the hole-punch test and the tensile stretchability test to consider the cause of shearing-induced damages (e.g., plastic strain and voids). See Figure 2 for examples. These models are under final validation against new experimental data for the two selected steels. Interim results from the modeling indicate that phase strength disparity can be a primary factor in determining the amount of shearing-induced damage near the edge. Once validated, the computational models are expected to improve the understanding of key factors influencing edge stretchability in DP980 steels.

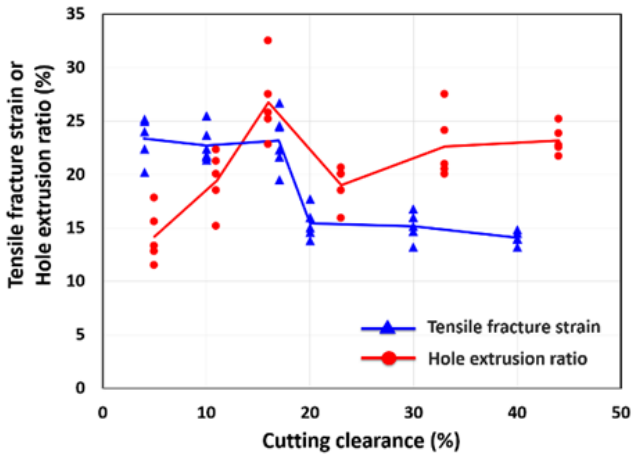

Figure 1. Effects of cutting clearance on tensile fracture strain and hole extrusion ratio in DP2 steels.

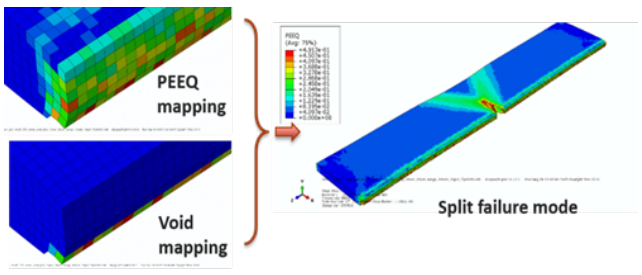

Figure 2. Predicting the macroscopic tensile stretchability with considerations for shearing-induced damage.

2017 U.S. DRIVE Highlight

Predictive Engineering Tools for Injection-Molded Long-Carbon-Fiber Thermoplastic Composites

Pacific Northwest National Laboratory validates and improves tools for predicting component performance to enable expanded use of lightweight carbon fiber composites in vehicles.

Pacific Northwest National Laboratory

Pacific Northwest National Laboratory (PNNL) led a team consisting of an automotive original equipment manufacturer (OEM), Tier 1 suppliers, a software developer, and three universities in an effort to integrate, optimize, and validate fiber orientation and length distribution models previously developed and implemented in a commercial software package for injection-molded long-carbon-fiber (LCF) thermoplastic composite structures.

The ability of the advanced software package to predict fiber orientation and length distributions in LCF/polypropylene (PP) and LCF/polyamide-6,6 (PA66) plaques was successfully demonstrated to within 15% of experimental results. The team investigated LCF loadings of 30 and 50 weight percent along with two contrasting injection speeds and two plaque injection geometries, edge-gated and center-gated. Software package improvements decreased computation time and reduced required memory for the fiber length calculation by 61%.

The team selected a representative automotive part with complex three-dimensional (3D) geometry, including variations in wall thickness and mold flow direction, to further validate the model. The part was injection-molded from LCF/PP and LCF/PA66 materials in both ribbed and non-ribbed variants. The advanced software package developed successfully predicted fiber orientation and length distributions at key locations in the complex part within 15% of experimental results.

Working with the OEM and Tier 1 partners, the team estimated weight savings using software predictions and structural analysis at 43% weight reduction for the part made from LCF/PA66 relative to that same part stamped in 1 mm gauge steel. The validated model has been included in revisions to the commercial software.

The project validation used an existing component, identified by the OEM, with requisite complex features, including change in molding flow direction and variation in wall thickness, and select material options. With the successful demonstration and use of the developed software improvements, the commercially-available software may now confidently be used to predict stiffness performance in additional components molded and material sets. This new tool will allow designers to estimate component performance without having to build molds, mold parts, and test parts to evaluate every potential design and, ultimately, should lower barriers to using carbon-fiber reinforced plastics on vehicles, thus enabling lightweighting. The validated software tools can be used to optimize a part by comparing the relative performance of variations in part design and materials, however part optimization was not in the scope of this project.

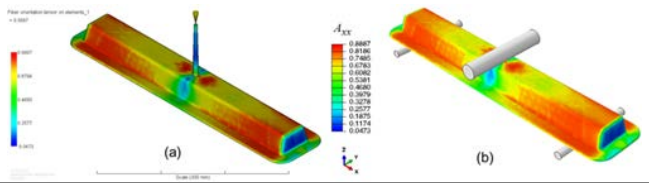

Figure 1. Fiber orientation prediction in 3D complex part using commercial software (left) before importing into the PNNL-developed model (right) for stiffness performance prediction.

Figure 2. Mold fill profiles of the 3D complex part.

2017 U.S. DRIVE Highlight

Low-Cost Magnesium Sheet Component Development and Demonstration Project

With the goal of developing new technologies that enable safe, minimum mass vehicle designs, USAMP has collaborated extensively on research with academia, material suppliers, and technology vendors to accelerate the development of low-cost advanced magnesium alloys and sheet forming technology.

U.S. Automotive Materials Partnership

The objective of this new project is to research, develop, and demonstrate at least one large, challenging magnesium (Mg) sheet component on a model year 2013 or newer vehicle at a manufacturing cost of less than $2.50 per pound of weight saved. To accomplish this, the U.S. Automotive Materials Partnership (USAMP) will research, develop, test, and evaluate at least one Mg alloy and commensurate processing configuration(s) suitable for rolling thin, automotive appearance grade sheet, and forming door inner and outer panels based on the 2013 Ford Fusion (see Figure 1) to validate the results of the effort.

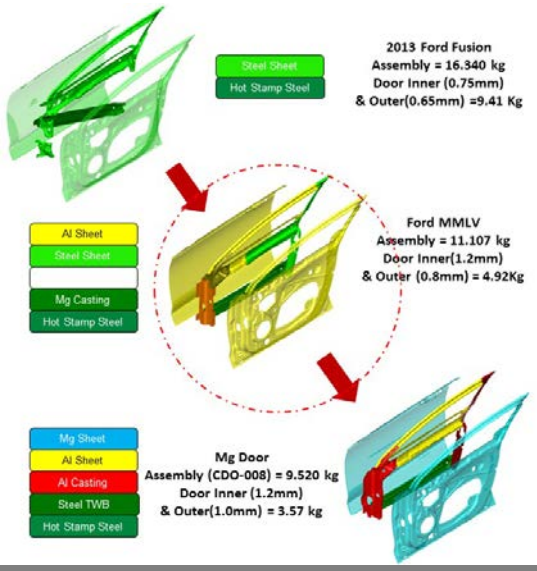

Figure 1. 2013 Ford Fusion door progression from baseline steel door, through aluminum intensive door, through aluminum intensive door with Mg inner and outer panels.

The three-year project consists of technical cost guidance to identify key cost drivers associated with: current Mg component production; material characterization and modeling studies; rolling trials on ingots; pretreatment, coating application, and lubrication studies; forming studies and scaling to large components; and joining studies. The project team will curate and host public data and code developed as part of the project in a repository that the LightMAT consortium developed and maintains.

During Year 1, USAMP organized a project team of 16 subrecipients and vendors and then held regular technical review meetings. USAMP also provided baseline commercial ZEK100 sheet material to all partners for characterizing and testing of mechanical properties and manufacturing processes. USAMP initiated a technical cost guidance study to identify key Mg door panel production process cost drivers and to establish a baseline steel door reference cost for comparison to the Mg components at the end of the project. The team has proposed three experimental alloys for integrated computational materials engineering (ICME) model calibration studies, detailed properties characterization, and sheet processing studies, as well as for evaluating formability properties during Budget Period 2. The team also identified and contracted key vendors to supply commercial and experimental Mg sheet alloys, and ingots from three unique Mg alloys proposed by the USAMP team. Finally, project industrial partners initiated experimental studies on Mg sheet coatings, pretreatments, and forming lubricants to identify the best approaches and processing conditions for treating coils and components intended for automotive component production environments.

The value of this project to original equipment manufacturers lies in the potential availability of at least one lower cost, more formable Mg sheet alloy. The reduced cost of using Mg sheet in automotive applications is due to (a) improved formability at reduced temperatures and (b) improved corrosion protection and reduced coating costs as a result of improved forming lubricant and coating technologies, thus enabling substantial mass reductions at reduced cost compared to today.

CROSSCUTTING

Codes and Standards

2017 U.S. DRIVE Highlight

Fuel Cell Electric Vehicle Tunnel Accident Safety Concerns Addressed through Scenario Modeling

National laboratories team delivers risk assessment, computer modeling, and emergency response education to address the concerns of authorities having jurisdiction about fuel cell electric vehicles in tunnels.

National Renewable Energy Laboratory, Pacific Northwest National Laboratory, and Sandia National Laboratories

A team from the U.S. Department of Energy and national laboratories successfully evaluated fuel cell electric vehicle (FCEV) tunnel accident scenarios, quantified potential impacts on tunnel structure, and alleviated concerns from authorities having jurisdiction (AHJs) about tunnels in the Northeastern United States. This Northeastern area, stretching from Washington, DC to Boston, includes heavily used vehicle tunnels, the use of which will be critical to successful FCEV deployment. Questions and concerns voiced by the AHJs led to a project to define and assess specific accident scenarios.

Beginning with possible accident scenarios, the team conducted a risk analysis to determine the likelihood and consequences of each specific case. The risk analysis determined that the most likely consequences of a crash would fall within tunnel design limits and therefore not endanger the tunnel's structural integrity. Scenarios included vehicle fire events, as well as minor crashes and a variety of scenarios in which hydrogen (H_2) is not released or is diluted safely. One scenario identified for in-depth study involved an overturned FCEV that was exposed to a hydrocarbon fire, with a jet fire ensuing as H_2 is vented from the tank. The scenario was modeled for two actual tunnels to predict the thermal expansion of the steel in the tunnel structure and the temperature of the ceiling where the H_2 jet flame would impinge (Figure 1).

The conclusions from the modeling were that the tunnel's steel structure would not be compromised by the impingement of the H_2 jet fire, though temperatures in the ceiling were calculated to be high enough that concrete damage may occur in the area where the H_2 jet flame impinges if there is no ventilation. If ventilation is operating, the maximum temperature is significantly lower and concrete damage is not expected to occur. The team conducted a final analysis to determine whether the steel structure supporting the overhead concrete panels would reach the epoxy melting temperature of 140°C, thereby compromising its anchor points. The analysis concluded that the H_2 flame duration is too short to increase the steel temperature to the epoxy melting point.

The team also compiled and tailored emergency response guidance to the AHJs' interests. This guidance, along with the report documenting the results of the risk analysis and computer modeling, was delivered to AHJs in the Northeast. The report, along with outreach meetings, have improved the way AHJs view FCEVs, and AHJs have expressed interest in learning more and in moving forward on the path to approval of FCEVs in tunnels.

The report will be incorporated by reference in the NFPA 502 Standard for Road Tunnels, Bridges, and Other Limited Access Highways 2021 edition. Incorporating this analysis into NFPA 502, the most widely-used safety standard for tunnels, should reduce the effort required for future FCEV tunnel approvals.

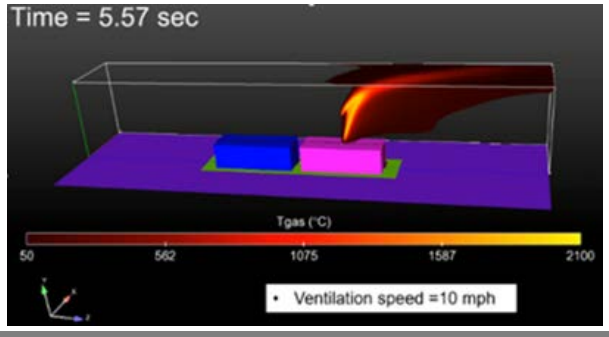

Figure 1. A model of the H_2 jet hot gas mixture where the tunnel enclosure has a ventilation of 10 mph.

Grid Interaction

2017 U.S. DRIVE Highlight

Minimizing Negative Impact of Electric Vehicle Charging on the Electric Grid

Idaho National Laboratory researchers developed test procedures to understand how plug-in electric vehicles respond in real-world adverse electric grid conditions. These results inform all stakeholders and drive the SAE J2894 standard on power quality requirements.

Idaho National Laboratory

As sales of plug-in electric vehicles (PEVs) rise, so too do concerns that PEV charging systems might impact the electric grid. In order to better understand how PEV charging might impact the grid, over the past decade Idaho National Laboratory (INL) research engineers have developed test procedures to characterize how PEVs behave as loads on the grid when using alternating current (AC) Level 1, AC Level 2, and direct current (DC) fast charging systems. Taken together, these testing procedures cover a wide variety of possible situations. Some tests characterize the steady-state charging behavior of the PEV charger to include charger efficiency, power factor, and the harmonic distortion in the current as a function of charge rate. Other tests characterize the PEV charger's dynamic response to a wide variety of adverse grid conditions such as voltage distortion, momentary outages, voltage, and frequency deviation.

This research has produced valuable results, including identification of potential issues with PEV charging that were not initially obvious. A case in point: Researchers observed the constant power behavior of some PEV chargers to create current spikes during a voltage sag event. Figure 1 shows the response of three commercially-available PEVs to a voltage sag (drop) of 240 volt (V) to 100 V lasting 0.05 seconds. During the sag, the on-board charging module on each PEV responds differently, with the level of current drawn by two of the PEVs increasing substantially (but in different amounts) while the third PEV stops charging altogether. Each response is non-ideal and each could pose stability problems to the grid. Discovery of this behavior has prompted further investigation to understand ramifications and identify counter-measures.

As a second example, INL characterization results have also proved valuable in determining how the PEV charge rate is linked to charging efficiency and the harmonic distortion in current.

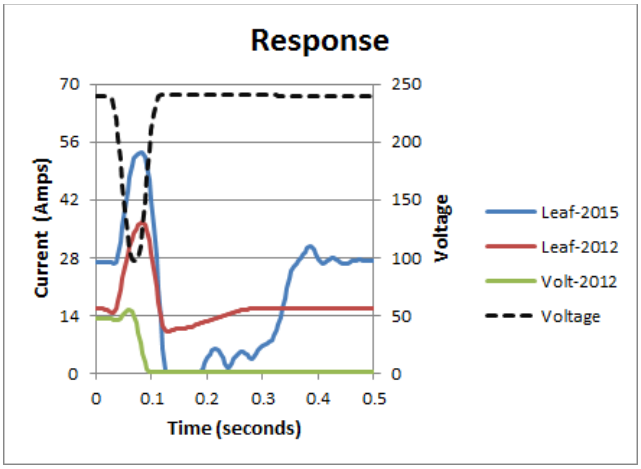

Figure 1. The response to a voltage sag of three production PEVs. In this test, the voltage drops from 240 V to 100 V for 0.05 seconds. The large increase in current of two of the PEVs during the voltage sag is undesirable.

SAE International and its industry affiliates have benefited from the PEV characterization work at INL. The SAE J2894 Power Quality Requirements for Plug-In Electric Vehicle Chargers subcommittee is developing a set of recommended practices designed to ensure that PEV on-board charging modules are capable of functioning without causing problems for the electric grid and can function properly in non-ideal grid conditions. INL's characterization results are a core resource for the subcommittee, because they brought to light previously unknown issues. Data provided by INL are necessary to define robust parameter limits in the recommended practices that prevent these issues.

2017 U.S. DRIVE Highlight

Smart Workplace Charging Reduces Electricity Cost for Electric Vehicles at Commercial Facilities

Development of a smart charging management system that is integrated with facility meters can avoid demand charges through peak load management and reduce the cost of electricity for workplace charging.

National Renewable Energy Laboratory

The National Renewable Energy Laboratory (NREL) has developed a smart charging control system to aggregate plug-in electric vehicle (PEV) charging that reduces the cost of electricity for the rate payer at workplace or commercial facilities. In some cases, the electricity for these facilities are billed for the energy consumed (kWh) or energy charge, and a demand charge, which is the peak power (kW) or rate energy is consumed during the billing period.

The demand charge portion separately reflects the infrastructure cost associated with serving peak load periods. As a result, energy charge rates are less for commercial facilities with demand charges than those without demand charges in the same service territory. An analysis of workplace charging at the National Renewable Energy Laboratory (NREL) has shown that reduced charging during critical periods could decrease the annualized average cost of charging from about 10¢ per kWh to as low as 3.8¢ per kWh. This reduction is possible because the peak net load for the rest of the NREL load "behind-the-meter" tends to occur in either the early morning or late afternoon. This smart charging control system can reduce the volatility of the marginal demand charge (see Figure 1) by leveraging the flexibility of when PEVs are charged.

These demand charges totaled $4,500, which could have been avoided through peak load management.

The smart charging control system asks PEV drivers to provide the required number of miles that need to be charged to reach their next charging destination, and when they plan to depart their current location. This information is used to schedule the charge of the connected vehicles such that their charging is not coincident with the expected demand peak of the facility and to ensure that the driving range needed by the PEV users is provided. Flexibility in charging time allows the system to reduce the PEV load during peak facility load periods (see Figure 2).

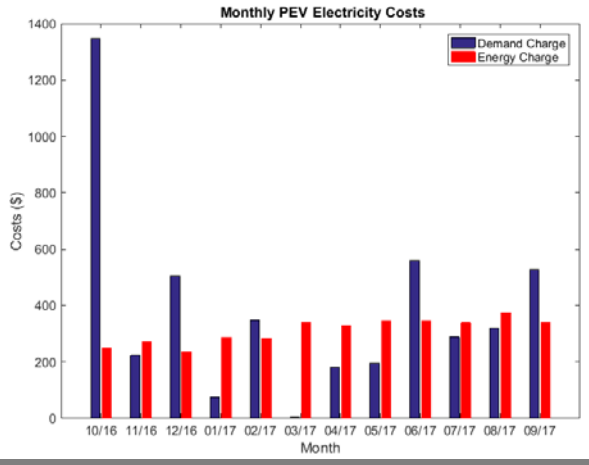

Figure 1. Monthly electricity cost of workplace charging at NREL where demand charges are on the margin for charging demand.

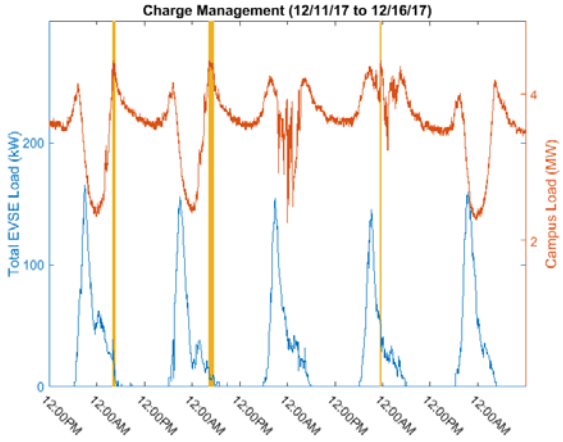

Figure 2. Smart charging control system reduces total PEV load during peak facility load periods (highlighted in yellow).

NREL has operated this system since January 2017 and will use the data collected for further development of predictive control. This control will help evaluate user's energy requirements and provide improved charge planning.

Hydrogen Storage

2017 U.S. DRIVE Highlight

Improvement of Metal Hydride Kinetics through Nanoconfinement Strategies

Elucidating metal-hydrogen reactions at nanointerfaces through high-performance computing has yielded enhanced performance and improved mechanistic understanding.

Hydrogen Materials—Advanced Research Consortium

Researchers have doubled the rates of hydrogen (H_2) uptake and release in a nanoconfined Li-N-H system. Lithium nitride (Li_3N) is a promising H_2 storage material with a theoretical gravimetric density upon hydrogenation of 10.4 wt% H_2, well above U.S. Department of Energy onboard storage targets. However, its use as a practical storage material is hindered by a slow two-step hydrogenation pathway, involving the formation of an intermediate phase, lithium imide (Li_2NH), which requires high reaction temperatures and long charging times. By confining Li_3N particles within nanoporous carbon structures, researchers at Sandia National Laboratories (SNL) and Lawrence Livermore National Laboratory (LLNL), each members of the Hydrogen Materials–Advanced Research Consortium (HyMARC), discovered that hydrogenation and dehydrogenation rates increased by a factor of two relative to bulk Li_3N.[1] Subsequently, the team used a combination of experiment and high-performance computing simulations to improve mechanistic understanding of the processes that cause this enhancement.

Further investigation using several HyMARC experimental and computational resources clarified the features of the observed rate enhancement. Experimentally, there was no evidence of the Li_2NH intermediate phase formation during reaction of the nanoconfined material (Figure 1) and computational modeling explained how nanoconfinement of the material avoided the formation of this intermediate. Molecular dynamics modeling showed that the thermodynamic factors responsible for the creation and growth of the Li_2NH intermediate become unfavorable as the particle size decreases. This occurs because interfaces that form within the solid with the intermediate phase carry an energetic penalty that increases as the particle size decreases. Keeping the particle size below a certain threshold value avoids Li_2NH formation, and allows the reaction to proceed in one step and at a higher rate.

This work provides practical guidance on how to design improved H_2 storage materials. These improved and experimentally validated computational models establish the importance of controlling nanointerfaces in solid-state H_2 storage reactions and introduce a new paradigm for enhancing performance by controlling the nanostructural architecture.

SNL and LLNL utilized several unique and complementary capabilities in this work. Now entering year three, HyMARC has made significant progress in foundational understanding of key phenomena governing the thermodynamics and kinetics of H_2 storage processes that have been impeding the development of practical H_2 storage materials for transportation applications.

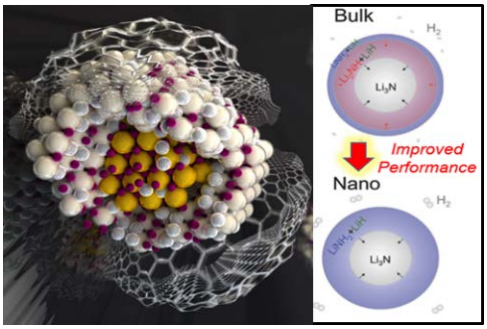

Figure 1. Left: schematic showing 1-step phase transition between Li_3N core and $LiNH_2$ + LiH outer shell during (de)hydrogenation (Li–purple, H–small white, N–yellow and large white spheres, nanoporous carbon–hexagonal net). Right: schematic showing difference between 2-step bulk and 1-step nanoconfined (de)hydrogenation reactions.

[1] Wood, B. C., et al., *Adv. Mater. Int.* 2017, *4*, 1600803.

2017 U.S. DRIVE Highlight

Computational Discovery & Experimental Confirmation Leads to Higher Capacity Hydrogen Adsorbents

Metal organic framework adsorbents with a rare combination of high volumetric and gravimetric densities of stored hydrogen were identified computationally and demonstrated experimentally.

University of Michigan and Ford Motor Company

A first-of-its-kind approach providing a holistic assessment of materials for onboard hydrogen (H_2) storage has identified overlooked adsorbents that surpass the state-of-the-art material, metal organic framework (MOF)-5. This approach employs a combination of high-throughput computation, experimental synthesis and characterization, and system-level modeling to identify H_2 adsorbents with potential of achieving U.S. DRIVE H_2 storage targets. The team's approach demonstrated the power of computational screening in guiding experimental efforts towards promising materials, and in doing so, established a new benchmark for volumetric hydrogen density in MOFs.

A high-capacity, low-cost method for storing H_2 fuel remains a barrier to the widespread adoption of fuel cell electric vehicles (FCEVs). Current storage systems are based on pressurized H_2 gas, which is bulky, expensive, and operate at high pressures. Consequently, alternative lower cost storage strategies with the potential for higher capacity and lower pressure are desirable. Of these, adsorbents such as MOFs present a promising approach due to their moderate operating pressures, fast kinetics, reversibility, and high gravimetric densities.[1]

Although several MOFs are known to exhibit high H_2 densities on a gravimetric basis, achieving high volumetric capacities remains a challenge for maximizing the driving range of FCEVs. Researchers from the University of Michigan and Ford have used high-throughput computational techniques to identify MOFs that simultaneously achieve high gravimetric and volumetric H_2 capacities, while outperforming the benchmark MOF-5 material.[1] Using simulations, researchers estimated the H_2 capacities of over 5,000 MOFs drawn from databases of known compounds. These screening results provided a fast and comprehensive assessment of adsorbent performance for H_2 storage.

Researchers subsequently synthesized and experimentally demonstrated the materials projected to have the highest potential. Consistent with the computational predictions, several compounds, including IRMOF-20 and SNU-70, exhibited a rare combination of high usable volumetric and gravimetric capacities. Importantly, the measured capacities exceeded those of the benchmark compound MOF-5, the previous record-holder for combined volumetric/gravimetric performance (Figure 1). To complete the new material evaluation, researchers incorporated the material-level experimental data into a full-scale storage system model to project performance with respect to U.S. DRIVE targets at the system level.

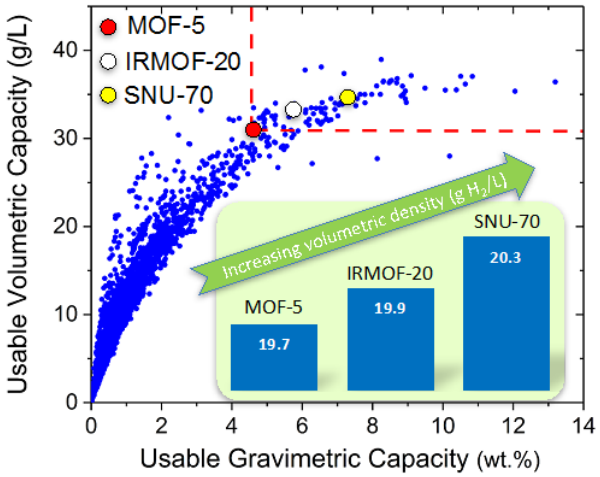

Figure 1. Usable volumetric vs. gravimetric H_2 storage capacities predicted for over 5,000 MOFs. The inset projects the improvement in volumetric performance at the system level.

[1] Ahmed, et al., *Energy Environ. Sci.*, 2017, 10, 2459-2471.

Integrated Systems Analysis

2017 U.S. DRIVE Highlight

Combined Heat and Power, and Carbon Capture and Storage Technologies, Reduce Greenhouse Gas Emissions from Power Generation

A life-cycle environmental analysis of coal and natural gas power generation technologies.

Integrated Systems Analysis Technical Team

Domestic coal and natural gas (NG) are abundant and low-cost energy sources. According to the U.S. Energy Information Agency, approximately two-thirds of the electricity supplied t0 the U.S. grid (2,600 TWh) in 2016 was generated from these two energy sources (1,200 TWh from coal and 1,400 TWh from NG). However, using these fossil sources for power generation produce emissions that may adversely impact the environment. Using coal and NG for grid power generation produced 1.3 and 0.7 billion metric tons of life-cycle CO_2e,[1] respectively, for a combined 2 billion metric tons of greenhouse gas (GHG) emissions in 2016.

The Integrated Systems Analysis Technical Team (ISATT) evaluated technology pathway options that reduce GHG emissions associated with using fossil coal and NG for power generation. The evaluated technology options include combined heat and power (CHP) generation, and post-combustion carbon capture and storage (CCS) technologies. ISATT expanded Argonne's Greenhouse gas, Regulated Emissions, and Energy use in Transportation (GREET®) model to conduct life-cycle GHG emissions analysis of fossil-based power generation technologies. The evaluated power generation technologies for CHP and CCS are steam turbine, combined cycle, and fuel cells powered by NG, and steam turbine powered by coal. The life-cycle analysis in GREET for these technology pathways includes energy use and emissions associated with coal and NG extraction, processing and transportation to power plant, conversion to electricity (and heat for CHP plants), heat and electricity needed for CCS, as well as transmission and distribution of generated electricity.

Figure 1 shows the life-cycle GHG emissions of U.S. average electricity generation mix in 2016 and for individual coal and NG power generation technologies, including the CHP and CCS technology options. The U.S. average generation mix produced GHG emissions of 540 gCO_2e/kWh, while coal, NG steam, NG fuel cell and NG combined cycle produced 1,080, 770, 570 and 470 gCO_2e/kWh, respectively. The CHP technology options reduce GHG emissions by 250 and 270 gCO_2e/kWh for coal and NG steam turbine generation technologies, respectively, and by 310 and 90 gCO_2e/kWh for the NG fuel cell and combined cycle technologies, respectively. Integrated CCS technology reduces GHG emissions by 860 gCO_2e/kWh when applied to coal steam turbine technology and 340 gCO_2e/kWh when applied to the low-emitting NG combined cycle technology. The study shows that GHG emissions associated with fossil-based power generation technologies can be significantly reduced by utilizing byproduct heat from thermal and fuel cell power cycles, and by employing CCS technologies with fossil power generation technologies.

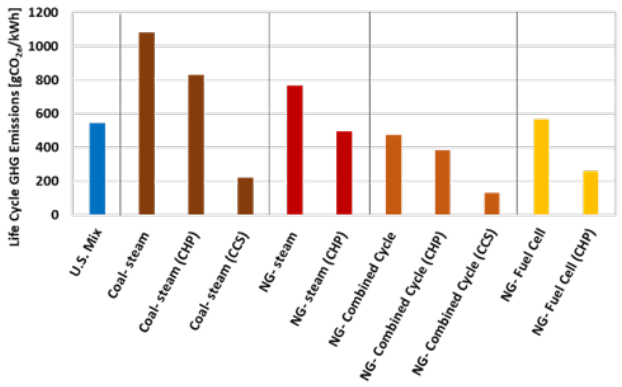

Figure 1. Life-cycle GHG emissions of coal and NG power generation technologies.

[1] Carbon dioxide equivalent of greenhouse gases.

2017 U.S. DRIVE Highlight

Cross-Study Comparison of Marginal Abatement Cost of Carbon Underscores Need for Independent, Transparent, Peer-Reviewed Studies

A meta-analysis of MAC for transportation and other sectors reported in recent key publications.

Integrated Systems Analysis Technical Team

In 2016, Argonne National Laboratory (ANL) published a report documenting "Cradle-to-Grave Lifecycle Analysis of U.S. Light-Duty Vehicle-Fuel Pathways: A Greenhouse Gas Emissions and Economic Assessment of Current (2015) and Future (2025–2030) Technologies." This provided a comprehensive cradle-to-grave (C2G) analysis of greenhouse gas (GHG) emissions, levelized cost of driving, and cost of avoided GHG emissions of a variety of vehicle-fuel technology pathways. To provide additional context for the report's findings and to understand how its conclusions compare with those of other published analyses, the Integrated Systems Analysis Technical Team (ISATT) of the U.S. DRIVE Partnership performed a systematic comparison of the marginal abatement cost (MAC) of carbon across studies and energy sectors.

ISATT performed the cross-sector analysis by conducting a literature review, cataloguing reported sector and subsector's emissions and costs. Publications considered in this analysis included: "Reducing U.S. greenhouse gas emissions: How much at what cost?" (McKinsey, 2007 and revised 2009); "Analysis of Measures to Meet the Requirements of California's Assembly Bill 32" (Stanford, 2008); "U.S. MAC Curve: A Fresh Look at the Costs of Reducing U.S. Carbon Emissions" (BNEF, 2010); "Annual Energy Outlook 2014" Reference Case, and Greenhouse Gas $10 and $25 Side Cases (EIA, 2014); and "Integrated Fuels and Vehicles Roadmap to 2030" (Roland Berger, 2016).

The comparison revealed major differences and a lack of transparency of key assumptions and methodology across studies, which underscored the need for independent, transparent, peer-reviewed studies that allow replication of results by other independent researchers.

A wide range of MAC values are reported between and within studies, covering a breadth of assumptions, scope, methodologies, regions, and timeframes. ISATT conducted a sensitivity analysis of baseline technology selection (against which the alternatives are compared), vehicle incremental cost, and oil price assumptions in ANL's 2016 C2G report to highlight the importance of those key assumptions. In MAC terms, vehicle efficiency improvement is the least expensive, followed generally by hybridization, biofuels, and electrification/fuel cells. However, it is important to recognize that efficiency improvements and hybridization may not provide deep carbon emissions reductions. These observations come with caveats, given the multitude of input assumptions and the associated lack of transparency. Each study's conclusions should be digested independently within its scope, region, assumptions and timeframe. Thus, conclusions from any given study are not directly comparable with other studies, suggesting that intra-study cost comparisons are most appropriate.

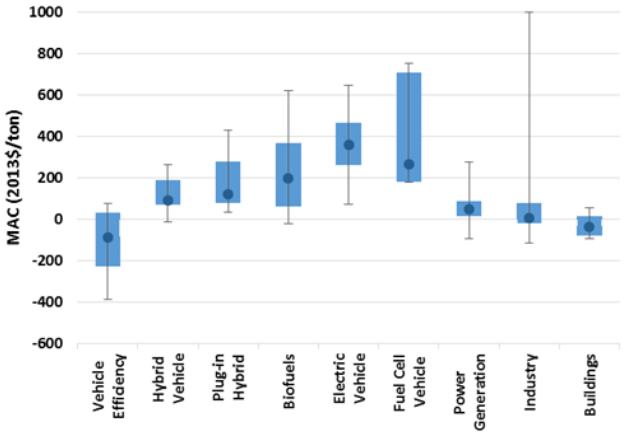

Figure 1. Ranges of MACs reported by key publications for transportation technologies and other economic sectors. Boxes show the 25%–75%ile range; whiskers show the min-max range.

FUELS

Fuel Pathways Integration

2017 U.S. DRIVE Highlight

Analysis of Hydrogen Fuel Pathways Confirms Need for Further Research to Reduce Hydrogen Cost

In the modeled scenario, hydrogen produced via natural gas reformation—either on-site or centrally with pipeline or truck delivery—offers the lowest fuel costs and low greenhouse gas emissions.

Fuel Pathway Integration Technical Team

The Fuel Pathway Integration Technical Team (FPITT) reviewed the U.S. Department of Energy's (DOE) preliminary evaluation of eight advanced-technology hydrogen production, delivery, and distribution pathways, providing industry perspective. DOE's Fuel Cell Technologies Office analyzed the lifecycle cost, energy use, and greenhouse gas emissions performance of these eight hydrogen fuel pathways. The analysis utilized up-to-date, publicly available models to estimate the costs and performance of hydrogen technologies anticipated to be available in 2025. The assessment complements DOE's 2013 hydrogen pathways evaluation of currently available hydrogen technologies and incorporates data and modeling from the U.S. DRIVE's Cradle-to-Grave (C2G) lifecycle assessment of advanced vehicle-fuel technologies, expanding the number of C2G hydrogen fuel pathways investigated.[1]

The 2017 pathway evaluation includes costs (in 2016 dollars) for hydrogen production, delivery, and refueling station compression, storage, and dispensing. It found that the costs associated with the advanced-technology pathways studied exceeded DOE's $4/kg hydrogen research and development cost target, indicating the need for further research and development to reduce the pathway costs. The levelized costs of dispensed hydrogen from the eight pathways are estimated to be in the range of $4.40/kg to $7.40/kg, with distributed hydrogen production from natural gas reformation providing the lowest-cost hydrogen (see Figure 1).

In addition to the cost evaluation, FPITT's analysis included estimates of the greenhouse gas emission reductions for the advanced-technology pathways.

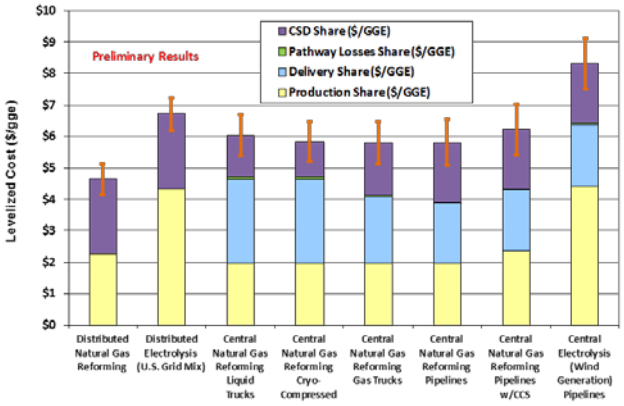

Figure 1. Preliminary dispensed hydrogen levelized cost (including cost of infrastructure) for eight advanced-technology pathways in dollars per gallon of gasoline equivalent (gge).

[1] See Ramsden, et al. (2013). *Hydrogen Pathways: Updated Cost, Well-to-Wheels Energy Use, and Emissions for the Current Technology Status of Ten Hydrogen Production, Delivery, and Distribution Scenarios*. National Renewable Energy Laboratory, Golden, CO. TP-6A10-60528; and Elgowainy, et al. (2016) *Cradle-to-Grave Lifecycle Analysis of U.S. Light-Duty Vehicle-Fuel Pathways.* Argonne National Laboratory, Argonne, IL, ANL/ESD-16/7.

2017 U.S. DRIVE Highlight

Completed Reassessment of Hydrogen Cost Target Using Systematic Probability Modeling

As a result of a recent probability analysis, the U.S. Department of Energy is considering an ultimate hydrogen R&D cost target of $4/gge on an untaxed basis as dispensed to the vehicle and an interim 2025 target of $7/gge.

Fuel Pathway Integration Technical Team

In 2017, the U.S. Department of Energy (DOE) comprehensively revisited the hydrogen (H_2) research and development (R&D) cost target using probability modeling. The analysis resulted in an ultimate H_2 R&D cost target of $4 per gallon of gasoline equivalent (gge, equivalent energy basis to a kilogram of H_2) (untaxed, delivered and dispensed to the vehicle, in 2016 dollars) and an interim H_2 cost target of $7/gge for 2025. The Fuel Pathway Integration Technical Team reviewed DOE's analysis methodology, assumptions, and data, providing an industry perspective. The cost targets are valuable for guiding H_2 and fuel cell R&D activities.

Researchers used Monte Carlo stochastic simulations to project the competitive conditions faced by H_2 fuel cell electric vehicles (FCEVs) in the 2020–2030 timeframe. The analysis assumed that FCEVs will compete with advanced internal combustion engine gasoline vehicles (ICEVs) in 2025 and, ultimately, with hybrid electric vehicles (HEVs). Researchers calculated the range of H_2 fuel costs under which consumers' costs to own and operate an FCEV (on a dollar-per-mile basis) could be competitive with gasoline ICEV ownership in 2025, and ultimately with HEV ownership. Researchers used probability distributions to calculate per-mile vehicle and fuel costs.

The analysis was pathway independent with respect to H_2 production and delivery technology options, and it reflected the variability in future fuel efficiency, competing gasoline fuel costs, and incremental vehicle purchase costs (see Figure 1).

The gasoline cost distribution was developed from the Energy Information Administration's 2017 Annual Energy Outlook (Reference and High- and Low-Oil Price cases for 2025). Distributions for vehicle fuel economy and incremental vehicle cost were based on data from the U.S. DRIVE Cradle-to-Grave lifecycle analysis of light-duty vehicles.[1] The 2025 H_2 R&D cost target of $7/gge and ultimate H_2 R&D cost target of $4/gge are based approximately on the 75th percentile results for H_2 cost compared to ICEVs and HEVs, respectively.

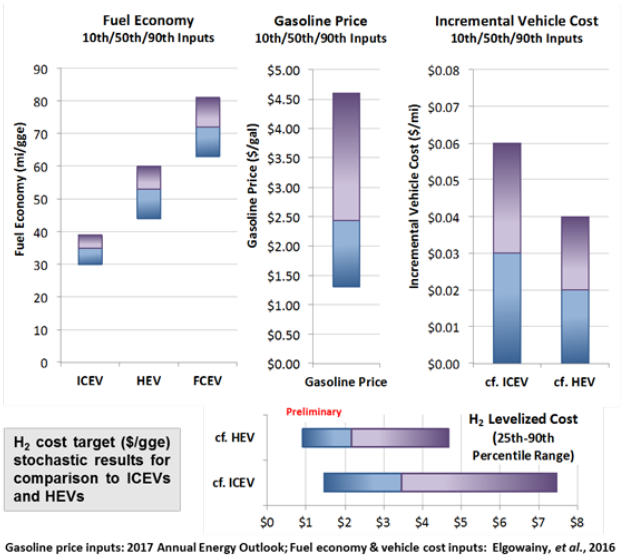

Figure 1. Input parameters (10th, 50th, and 90th percentiles) and fuel cost results for the H_2 cost stochastic analysis.

[1] See Elgowainy, et al. (2016) *Cradle-to-Grave Lifecycle Analysis of U.S. Light-Duty Vehicle-Fuel Pathways*. Argonne National Laboratory, Argonne, IL, ANL/ESD-16/7.

2017 U.S. DRIVE Highlight

Alignment of Next-Generation Vehicles and Fueling Infrastructure

Techno-economic analysis is identifying the largest contributors to the costs of owning fuel cell vehicles currently and in the foreseeable future, to inform research and development priorities and investments.

National Renewable Energy Laboratory and Argonne National Laboratory

The Fuel Pathways Integration Technical Team initiated the Hydrogen Interface Task Force (H2IT), a cross-cutting team of participants from various U.S. DRIVE hydrogen technical teams (Production, Delivery, Storage, and Codes & Standards) working to perform a holistic hydrogen pathway techno-economic analysis. The task force aims to understand the interfaces and tradeoffs between emerging hydrogen production, delivery, and onboard storage technologies. The team will determine which pathways exhibit the most favorable cost per mile and fuel cell electric vehicle (FCEV) performance (range, passenger/ cargo space, etc.). The team will also determine impact, identify transition and decision points, and develop implementation strategies and timelines for a transition from baseline 700 bar infrastructure to potential future hydrogen pathways in an effort to inform future research priorities.

The H2IT evaluated 700 bar onboard storage of hydrogen produced at a central production facility and delivered via either gaseous tube trailer or liquid tanker, assessing the cost of FCEV ownership (considering fuel costs and vehicle purchase cost less resale). The H2IT found that hydrogen delivery and dispensing account for about 20% of the cost of driving an FCEV over the lifetime of the vehicle (see Figure 1). In the initial three years of vehicle ownership, the hydrogen storage technology used onboard the FCEV accounts for about 10% of the cost of driving.

Cryo-compressed hydrogen storage (CcH2) can offer ~50% greater hydrogen density compared to traditional 700 bar storage and reduces the amount of equipment needed at the station. However, CcH2 requires energy-intensive hydrogen liquefaction, and the potential for boil-off losses for vehicles driven infrequently can be a challenge. Initial H2IT analysis found that the levelized cost of driving for the CcH2 pathway is equivalent to that for 700 bar onboard storage with liquid tanker delivery. Both liquid pathways have a slightly higher cost compared to 700 bar onboard storage with gaseous delivery, but they are preferable for larger station sizes and when longer delivery distances are required.

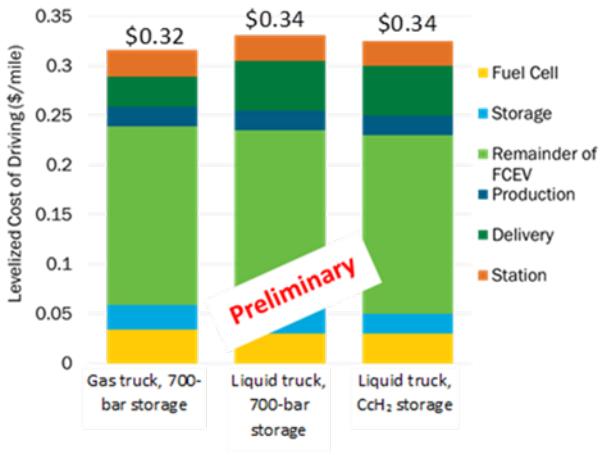

Figure 1. Levelized cost of driving for three hydrogen delivery and onboard storage pathways, assuming centralized hydrogen production via steam methane reforming, and economies of scale.

In 2018, H2IT will analyze the holistic (production, delivery, and storage) costs necessary for other forms of hydrogen storage, including cold-compressed and materials-based (adsorbents and metal hydrides), on a levelized cost of driving basis. The H2IT will also look at transition points and technical challenges to help inform U.S. DRIVE and the U.S. Department of Energy of necessary project portfolio focus areas.

Hydrogen Delivery

2017 U.S. DRIVE Highlight

Coatings to Enhance Reliability of Hydrogen Compressors

Proof-of-concept established for a coating process to enhance life of polymeric compressor seals.

GVD Corporation

GVD Corporation has utilized an innovative coating process that dramatically enhances the durability of seals used on compressors at hydrogen (H_2) fueling stations. H_2 compressors account for 15% of maintenance hours at stations, largely due to failure of seals. Causes of failure include high-temperature operation, fatigue of the seals under repeated pressure cycling, friction, and permeation of H_2 into the seal materials. GVD is utilizing an initiated chemical vapor deposition (iCVD) technology developed at the Massachusetts Institute of Technology to apply coatings to these seals that mitigate the latter two causes of failure. GVD's coatings improve seal lubricity, and mitigate H_2 ingress. In 2017, GVD completed proof-of-concept testing by coating a batch of seals and evaluating how much these seals eroded relative to uncoated seals when used for 875-bar H_2 compression. The loss of mass that GVD's coated seals experienced was over 70% less than that of uncoated seals (Figure 1), demonstrating a substantial improvement in durability. Additionally, preliminary results using helium gas indicate that their coatings reduce permeation of gas into compressor seals by 57%. GVD's ultimate goal from this project is to enhance the life of seals by 2X-4X.

The iCVD process consists of depositing alternating layers of coating material on a seal surface. The layers of coating serve two functions: 1) inorganic layers prevent H_2 ingress, and 2) polymeric layers enhance coating flexibility.

One benefit of the iCVD approach relative to other methods of vapor deposition is that it leverages an "initiator" species (i.e., catalyst) that allows the process to operate at room temperature; conventional processes require temperatures up to 700°C. The lower temperatures mitigate the negative impact that the deposition itself can have on coatings' structural strength and flexibility. GVD's coatings are expected to remain stable up to 200°C operating temperatures, the maximum temperature that H_2 compressors at fueling stations are expected to experience. Finally, the vapor deposition approach can be controlled to ensure that thin coatings (a few micrometers thick) are applied smoothly to conform to the surface of seals, minimizing defects.

In 2018 and 2019, GVD will develop a "tumbler" that can be used to coat their seals from all sides (360°), and evaluate both the life and permeation of H_2 in their coatings through testing with industry partners and at the National Renewable Energy Laboratory (NREL). Additionally, GVD will adapt their approach to enable coating seals used in H_2 dispensers to mitigate leaks during H_2 fueling. The low operating temperatures (-40°C) and rapid fluctuations in pressure experienced by H_2 dispensers will require modifications to GVD's coating compositions and deposition process.

GVD's project work on coatings for H_2 infrastructure has been funded by the U.S. Department of Energy's Small Business Innovative Research program. With funding from other federal agencies, GVD is now also exploring the viability of their approach for coating vehicle tires and subsea electronics.

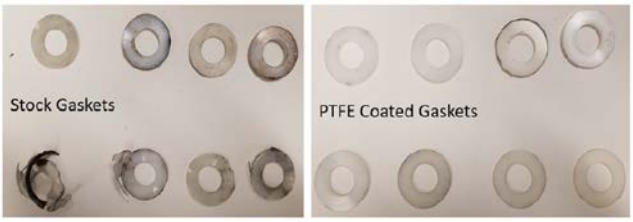

Figure 1. Performance testing at PowerTech and NREL has demonstrated a 70% reduction in seal erosion due to GVD's coatings.

2017 U.S. DRIVE Highlight

Computational Modeling of Hydrogen Effects in Steel

Advanced imaging, experimentation, and modeling techniques to guide development of novel steels.

Sandia National Laboratories, Oak Ridge National Laboratory, National Institute of Standards and Technology, Colorado School of Mines, and the University of Alabama

Sandia National Laboratories, Oak Ridge National Laboratory (ORNL), the National Institute of Standards and Technology, Colorado School of Mines, and the University of Alabama (UA) have initiated the development of a computational model that will correlate fundamental steel properties with real-world performance in hydrogen service. Key metrics of steels, such as strength or resistance to hydrogen effects, depend on many factors, one of which is believed to be microstructure. Steels are comprised of three-dimensional units known as "grains" which make up the microstructure. Grains can vary in size, shape, and phase based on chemical composition, steel processing, and deformation. A model that comprehensively integrates relationships between a steel's microstructure and its overall performance can expedite materials discovery and development, and is a long-term research goal in materials research.

In 2017, researchers at UA utilized an advanced imaging technique known as electron back-scatter diffraction to visualize the grain orientations and textures in a sample of high-strength (X100) steel, and characterize the microstructures of individual grains (Figure 1). This specimen's information was subsequently imported into the finite element modeling (FEM) software ABAQUS. Researchers are incorporating mechanical properties of the specimen into ABAQUS so that the software can be used to forecast the behavior of the steel given user-defined modifications, such as to microstructural constituents or grain boundary orientations.

One property measured in 2017 is each grain's "elasticity," or the reversibility of a material's response when it experiences a load. UA generated preliminary data for elasticity using nanoindentation, an approach wherein loads are applied to individual grains within a specimen and their response is measured.

Another property of interest is the steel's behavior in cyclic loading at a microstructural scale. Many applications used in hydrogen service today, such as pipelines and pressure vessels, experience fluctuations in pressure daily. These cycles (i.e., "fatigue") can generate damage in a material that ultimately causes cracks to grow. The damage level can vary depending on the amount of hydrogen that enters the steel from its environment. The research team will generate data for both of these properties in 2018. Researchers at UA will characterize the level of damage that the steels of interest incur under cyclic stresses. In parallel, researchers at ORNL will utilize their world-class high-pressure hydrogen chambers to characterize the rate at which hydrogen diffuses through specific steel microstructures.

The modeling work completed to date is a proof-of-concept demonstrating the ability to integrate advanced imaging techniques with FEM. As the model's functionality is enhanced, it can guide the engineering of novel steels optimized for service in hydrogen. The U.S. Department of Energy's Fuel Cell Technologies Office, and the U.S. Department of Transportation, jointly funded this effort.

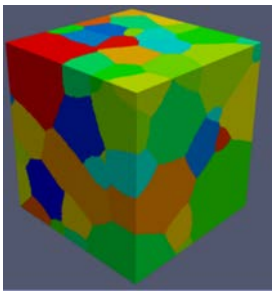

Figure 1. Visualization of individual grains of X100 steel in a finite element model. The grain boundaries depicted are nanometers in length.

2017 U.S. DRIVE Highlight

Mixed Refrigerants to Increase Efficiency of Liquefaction

World's first derived equations of state will allow for the use of "mixed refrigerants" in hydrogen liquefaction.

Washington State University and the National Renewable Energy Laboratory

Washington State University (WSU) and the National Renewable Energy Laboratory have derived equations of state (EOS) for two "mixed refrigerants" that can be used to improve the efficiency of hydrogen liquefaction. Liquefaction of any gas typically begins by "pre-cooling" the gas with a refrigerant. For example, when natural gas is liquefied, the refrigerant is typically a mixture of several different gases. The advantage of such "mixed refrigerants" over the use of a single gas is that the composition of a mixture can be optimized so that its rate of heating closely matches the cooling rate of the gas being liquefied; the closer the match, the more efficient pre-cooling will be.

Today, hydrogen liquefaction typically utilizes nitrogen as the refrigerant, rather than a mixture. This pre-cooling step accounts for 17% of the total exergy (i.e., available energy) used to liquefy hydrogen. Figure 1 shows the cooling curves of nitrogen, hydrogen, and a hypothetical mixed refrigerant (MR). The area between the curves represents the energy that is lost during liquefaction (i.e., inefficiency). In 2012, the European project "Integrated Design for Efficient Advanced Liquefaction of Hydrogen" (IdealHy) identified the need for mixed refrigerants to improve the efficiency of hydrogen liquefaction.

In 2017, WSU completed experimental measurements of the thermodynamic properties of mixtures of helium and hydrogen, as well as neon and hydrogen. WSU utilized the data generated along with other data in literature for these mixtures to derive EOS. These EOS characterize the pressures and temperatures of each of the mixtures across a broad range of temperatures; from near their critical points up to 300°K for the neon/hydrogen mixture, and up to 1,000°K for the hydrogen/helium mixture.

The EOS are now implemented in the National Institute of Standards and Technology's Reference Fluid Thermodynamic and Transport Properties (REFPROP) database.

The derivation of these EOS will enable the design of pre-cooling cycles and equipment that utilize mixed refrigerants to enhance the efficiency of liquefaction. Each of these refrigerants has unique benefits including: 1) the high molecular weight of neon, which can reduce the energy consumed in compression of a mixture; 2) the low boiling point of helium; and 3) the high thermal conductivity of hydrogen.

Remaining R&D needs to enable use of mixed refrigerants include: 1) additional experimentation to increase the number of mixture compositions (e.g., percent neon or helium) and cryogenic temperatures that the EOS can be applied to; and 2) development of liquefaction equipment (e.g., compressors) that can utilize these mixtures to generate cooling.

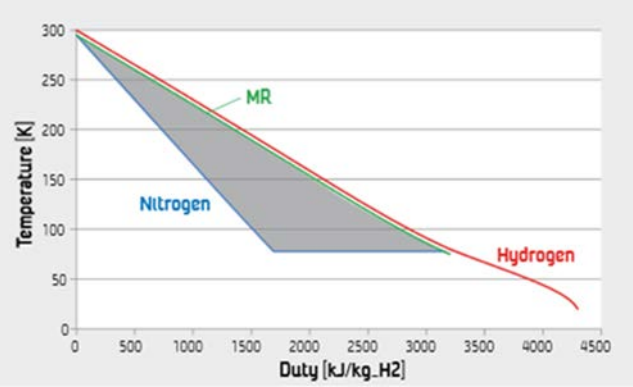

Figure 1. Cooling curves for nitrogen, hydrogen, and an ideal "mixed refrigerant" (MR). The area between two curves represents energy that is lost during liquefaction. Source: IdealHy, http://www.idealhy.eu/uploads/documents/IDEALHY_WHEC_2012_Poster_Mixed_Refrigerants.pdf.

Hydrogen Production

2017 U.S. DRIVE Highlight

HydroGEN Energy Materials Network Consortium

Accelerating research, development, and deployment of advanced water splitting materials for clean, sustainable hydrogen production via low- and high-temperature advanced electrolysis, photoelectrochemical, and solar thermochemical water splitting.

HydroGEN Consortium

As part of its Energy Materials Network (EMN),[1] the U.S. Department of Energy (DOE) established the HydroGEN[2] Consortium to accelerate discovery and development of advanced water splitting materials (AWSM) foundational to electrolytic, photoelectrochemical (PEC) and solar thermochemical (STCH) hydrogen (H_2) production pathways. These pathways offer sustainable, large-scale H_2 production utilizing diverse, domestic resources to split water, but suffer from significant materials challenges that limit their development and deployment. HydroGEN addresses these challenges by leveraging the extensive resources and expertise at DOE's national laboratories.

The HydroGEN Consortium includes six core national labs (Figure 1). HydroGEN experts collaborated in fiscal year (FY) 2016 to develop a compendium of "resource nodes" critical to water splitting technologies, focused on enabling viable commercial-scale H_2 production through state-of-the-art computational and experimental capabilities. In EMN terminology, a "resource node" is a unique national laboratory capability combining tools and techniques with well-established expertise, which is made accessible to the broader research community.

Within six months of its initiation, HydroGEN quickly established and made public through its website more than 80 resource nodes relevant to AWSM research. In addition, HydroGEN created templates for Non-Disclosure and Material Transfer Agreements and an Intellectual Property Management Plan to facilitate streamlined access to the consortium's capabilities by outside researchers.

By the end of FY 2017, 19 new projects were competitively selected and awarded to collaborate with HydroGEN on innovative early-stage materials research and development in the areas of advanced electrolysis, PEC and STCH. These industry, academic, and national laboratory project teams are already leveraging more than half of the Consortium's resource nodes, including world-class capabilities in advanced theory and computation; combinatorial synthesis and high-throughput screening; comprehensive materials characterization; and benchmarking. The fundamental materials science knowledge being gained is expected to significantly accelerate development of advanced water splitting technologies capable of producing H_2 at a cost of less than $2/gallon gas equivalent (gge).[3]

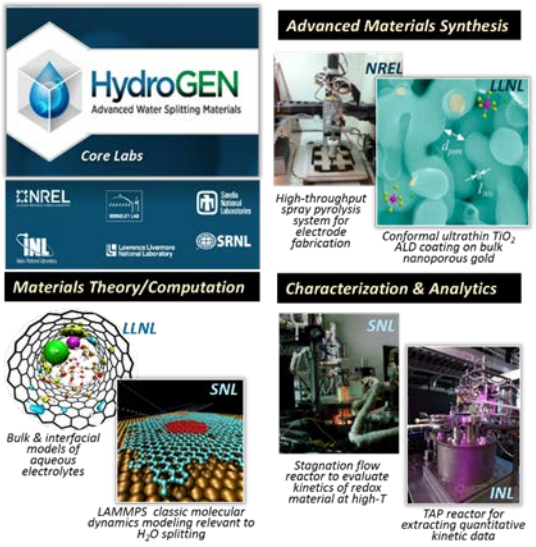

Figure 1. Example resource nodes available within HydroGEN fostering cross-cutting innovation using theory-guided applied materials R&D to advance emerging AWS pathways for H_2 production.

[1] The DOE EMN website: https://energy.gov/eere/energy-materials-network/energy-materials-network.

[2] HydroGEN Consortium on Advanced Water Splitting Materials website: https://www.h2awsm.org/.

[3] One gge is equivalent to 1 kg of H_2 based on energy content.

(This Page Left Intentionally Blank)